

The Three-Point Energy Correlator in the Coplanar Limit

Anjie Gao,¹ Tong-Zhi Yang,² and Xiaoyuan Zhang³

¹*Center for Theoretical Physics, Massachusetts Institute of Technology, Cambridge, MA 02139, USA*

²*Physik-Institut, Universität Zürich, Winterthurerstrasse 190, CH-8057 Zürich, Switzerland*

³*Department of Physics, Harvard University, Cambridge, MA 02138, USA*

E-mail: anjiegao@mit.edu, toyang@physik.uzh.ch,
xiaoyuanzhang@g.harvard.edu

ABSTRACT: Energy correlators are a type of observables that measure how energy is distributed across multiple detectors as a function of the angles between pairs of detectors. In this paper, we study the three-point energy correlator (EEEC) at lepton colliders in the three-particle near-to-plane (coplanar) limit. The leading-power contribution in this limit is governed by the three-jet (trijet) configuration. We introduce a new approach by projecting the EEEC onto the volume of the parallelepiped formed by the unit vectors aligned with three detected final-state particles. Analogous to the back-to-back limit of the two-point energy correlator probing the dijet configuration, the small-volume limit of the EEEC probes the trijet configuration. We derive a transverse momentum dependent (TMD) based factorization theorem that captures the soft and collinear logarithms in the coplanar limit, which enables us to achieve the next-to-next-to-next-to-leading logarithm (N^3LL) resummation. To our knowledge, this is the first N^3LL result for a trijet event shape. Additionally, we demonstrate that a similar factorization theorem can be applied to the fully differential EEEC in the three-particle coplanar limit, which provides a clean environment for studying different coplanar trijet shapes.

Contents

1	Introduction	2
2	Factorization in the coplanar limit	5
2.1	Kinematics	5
2.2	Factorization theorem	7
2.3	Ingredients	10
2.3.1	Hard Function	10
2.3.2	Jet function	13
2.3.3	Soft Function	14
2.4	Resummed formula	15
3	N^3LL resummation	16
3.1	Fixed-order expansion	16
3.2	Resummation	17
3.3	Scale uncertainties	20
4	Resummation for three gluon jets	21
5	Fully differential EEEC in the coplanar limit	24
6	Analysis	27
6.1	Non-perturbative corrections	27
6.2	Relation between D -Parameter and τ_p -projected EEEC	28
7	Conclusion	30
A	Running coupling and RG kernels	31
B	Anomalous dimensions	33
C	Fourier transformation	34
D	Fixed-order expansion	35

1 Introduction

The energy-energy correlation (EEC), which measures the energy deposited in two fixed detectors has recently attracted lots of attention in both perturbative QCD and collider physics. As pointed out in Refs. [1, 2], the EEC is a nice QCD observable because the soft gluon divergence is suppressed by the energy weights and the collinear divergence is regulated by the angle between the two detectors. More recently, EEC has been generalized to a new family of QCD observables called n -point *energy correlators* [3], defined as weighted cross sections in terms of the angles between any two of the final-state particles,

$$\frac{d\sigma}{dx_{12} \cdots dx_{(n-1)n}} \equiv \sum_m \sum_{1 \leq i_1, \dots, i_n \leq m} \int d\sigma_m \times \prod_{1 \leq k \leq n} \frac{E_{i_k}}{Q} \prod_{1 \leq j < l \leq n} \delta \left(x_{jl} - \frac{1 - \cos \theta_{ijil}}{2} \right). \quad (1.1)$$

Here m is the number of final-state particles and $d\sigma_m$ is the differential cross section for m final-state particles given a specific theory. The sum over i_1, \dots, i_n runs over all n subsets of the final states and the sum over m ensures the infrared safety due to Kinoshita-Lee-Nauenberg (KLN) theorem [4, 5]. We use the x_{ij} variables to label the angles between the detector i and j , which goes to 0 (or 1) when two detectors are collinear (or back-to-back). For $n = 2$, this definition reduces to the traditional EEC. For $n = 3$, namely the three-point energy correlator (EEE), the distribution encodes a non-trivial shape dependence that is associated with the QCD dynamics. This allows us to not only look at the shape of jets produced at colliders, but also probe the substructure inside a single jet.

For the past few decades, people have been dedicated to calculating scattering amplitudes at higher loops and understanding their mathematical structure. However, there are very few fixed-order data for the cross-section or collider observables. Monte Carlo simulations are preferred because the cuts from either phase space or jet algorithms make the integrals very complicated. Among these observables, energy correlators turn out to be the *simplest* one for analytic computation. For example, EEC has been computed to next-to-leading order (NLO) in QCD [6–8] and NNLO in $\mathcal{N} = 4$ super Yang-Mills (SYM) theory [9–12]. The leading order EEE with full angle dependence is then calculated in both QCD [13, 14] and $\mathcal{N} = 4$ SYM [15]. Very recently, the collinear limit of four-point energy correlator is also available [16]. On one side, the available fixed-order data allows us to push the precision for Standard Model measurements and new physics searches. On the other side, the analytic result reveals that there are various singular limits in the EEE distribution, including triple collinear limit ($x_{12}, x_{13}, x_{23} \sim 0$ homogeneously), squeezed limit ($x_{12} \sim 0$ and $x_{13}, x_{23} \sim x$), coplanar limit (three final-state particles fall onto the same plane), etc. These limits are summarized and the fixed-order expansions are provided in Ref. [13].

In perturbative quantum field theories, infrared divergences are always associated with large logarithms in some kinematic limits. Such logarithms could spoil the convergence of perturbation theory and one needs to resum them to all orders in α_s to retain the predictive power of perturbative expansions. At e^+e^- colliders, the EEC has been resummed to the next-to-next-to-leading logarithm (NNLL) accuracy [17, 18] in the collinear limit which is known as the Dokshitzer-Gribov-Lipatov-Altarelli-Parisi (DGLAP) region, and to N^4LL [19–27] in the back-to-back limit which is referred as the Sudakov region. At hadron colliders, the resummation of the transverse

EEC (TEEC) in the back-to-back limit has been pushed to N³LL accuracy [28, 29]. Regarding the EEEC, resummation becomes more subtle since there are multiple overlapping singular regions. To study the collinear limit, the simplest way is to project the full angular dependence into a one-dimensional space, namely the projected energy correlators [30]. The projected N -point correlator is defined as

$$\frac{d\sigma}{dx_L} = \sum_n \sum_{1 \leq i_1, \dots, i_N \leq n} \int d\sigma \frac{\prod_{a=1}^N E_{i_a}}{Q^N} \delta(x_L - \max\{x_{i_1, i_2}, x_{i_1, i_3}, \dots, x_{i_{N-1}, i_N}\}), \quad (1.2)$$

with x_L the largest angle, and logarithms of $\ln(x_L)$ in the collinear limit $x_L \rightarrow 0$ have been resummed to NNLL accuracy [31–33]. Very recently, this result was used by CMS collaboration to produce the most accurate α_s value from a jet substructure observable [34].

In this paper, we initiate the study of coplanar limit of energy correlators in the trijet region, where the three particles assigned with the energy weight fall almost on the same plane (see Fig. 1a). To access this limit, we introduce a *volume projection* of the EEEC (referred as τ_p -projected EEEC), defined as follows

$$\frac{d\sigma}{d\tau_p} = \sum_{h_1, h_2, h_3} \int d\sigma \frac{E_{h_1} E_{h_2} E_{h_3}}{Q^3} \delta(\tau_p - \tau_{h_1 h_2 h_3}), \quad \tau_{h_1 h_2 h_3} \equiv |(\hat{n}_1 \times \hat{n}_2) \cdot \hat{n}_3|. \quad (1.3)$$

Here h_1, h_2, h_3 run over all the final-state hadrons, and $\tau_{h_1 h_2 h_3}$ ¹ ranging from 0 to 1 is the volume of the parallelepiped formed by the unit vectors \hat{n}_1, \hat{n}_2 and \hat{n}_3 (as illustrated in Fig. 1b). Note that simply imposing $\tau_p \rightarrow 0$ is insufficient for infrared safety and selecting the interesting coplanar configurations. This is because $\tau_{h_1 h_2 h_3} \rightarrow 0$ also includes contributions where two particles are collinear (within one jet) or back-to-back (in the two different jets of the dijet configuration), or three particles are collinear (within one jet). To resolve this problem, we use the k_T (Durham) algorithm [35] to extract the coplanar trijet limit. Such a procedure was also used in some trijet analysis of event shapes [36, 37]. Explicitly, we impose a lower bound y_{cut} for the 3-jet resolution variable y_3 ² [35] to select coplanar three-jet events and modify the definition in Eq. (1.3) to

$$\left. \frac{d\sigma}{d\tau_p} \right|_{\text{trijet}} = \sum_{h_1 \in J_1} \sum_{h_2 \in J_2} \sum_{h_3 \in J_3} \int_{y_3 > y_{\text{cut}}} d\sigma \frac{E_{h_1} E_{h_2} E_{h_3}}{E_{J_1} E_{J_2} E_{J_3}} \delta(\tau_p - \tau_{h_1 h_2 h_3}), \quad (1.4)$$

where J_1, J_2, J_3 denote the three jets selected using the k_T algorithm, and $E_{J_1}, E_{J_2}, E_{J_3}$ are the energies of the three jets. Below we will focus on this particular definition (1.4), referred to as *the coplanar EEEC*, but omit the subscript “trijet”.

¹Although we take the absolute value in the definition of $\tau_{h_1 h_2 h_3}$, it is also interesting to explore $(\hat{n}_1 \times \hat{n}_2) \cdot \hat{n}_3$ without taking the absolute value, in order to study unconserved parity. In that case, the order of $\{h_1, h_2, h_3\}$ matters. One may consider ordering $\{h_1, h_2, h_3\}$ by the order of their energies, or by their azimuthal angles along a preferred direction. We leave the exploration of these possibilities to future work.

² y_3 is constructed as follows. Given a set of n momenta, for each pair of momenta (i, j) , calculate the distance variable of the k_T algorithm, $y_{ij} = 2 \min(E_i^2, E_j^2)(1 - \cos\theta_{ij})/Q^2$. Find the smallest y_{ij} and define it to be the n -jet resolution y_n . Combine such i and j into a single new pseudoparticle, with momentum $p = p_i + p_j$. Repeat this procedure until there are 3 (pseudo)particles left. Then y_3 is the 3-jet resolution of the remaining 3 (pseudo)particles.

To further analyze different coplanar configurations, we can also characterize the coplanar limit using celestial coordinates $\{s, \phi_1, \phi_2\}$ introduced in Ref. [15] and study the fully differential spectrum. As we will show in Sec. 5, the scaling variable s can access both the collinear limit ($s \rightarrow 0$) and coplanar limit ($s \rightarrow 1$), while values of $\phi_{1,2}$ fix specific shapes of the trijet. Since the factorization structure remains similar in either the τ_p definition or celestial definition, we will focus on the former case for the main part of this paper.

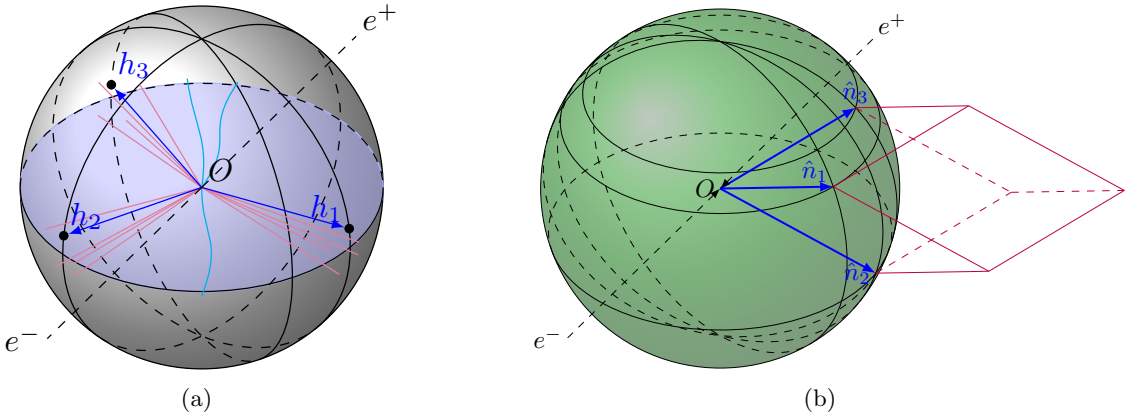


Figure 1: a) Configuration where h_1, h_2, h_3 are within three well-separated coplanar jets. b) Visualization for the τ_p projection of the EEEC. The three vectors \hat{n}_1, \hat{n}_2 and \hat{n}_3 represent the directions of three final-state hadrons h_1, h_2, h_3 , and they form a parallelepiped, whose volume defines τ_p .

The fixed-order expansion of the coplanar EEEC in perturbation theory can be written in the following form:

$$\frac{d\sigma}{d\tau_p} = \delta(\tau_p) \left[\left(\frac{\alpha_s}{4\pi} \right) A_1 + \left(\frac{\alpha_s}{4\pi} \right)^2 A_2 + \dots \right] + \left(\frac{\alpha_s}{4\pi} \right)^2 B(\tau_p) + \left(\frac{\alpha_s}{4\pi} \right)^3 C(\tau_p) + \dots . \quad (1.5)$$

Here, the delta function term arises from the three-particle configuration, where the three particles are exactly coplanar, and thus one has $\tau_p = 0$. The leading order (LO) distribution with non-trivial τ_p dependence, $B(\tau_p)$, starts at $\mathcal{O}(\alpha_s^2)$ with four-particle final states, and can be computed using the analytic EEEC result [13], or numerically using, e.g. Event2 [38, 39] and NLOJet++ [40]. The NLO contribution $C(\tau_p)$ including tree-level five-particle final states and one-loop four-particle final states, can also be computed by NLOJet++. Similar to the back-to-back limit of EEC, the coplanar EEEC receives double logarithmic series, i.e. $\frac{d\sigma}{d\tau_p} \sim \sum_k \sum_{l \leq 2k-1} \alpha_s^k \left(\frac{\ln^l \tau_p}{\tau_p} \right)_+$, which requires resummation to all orders. In this work, we will develop a factorization formula for the coplanar EEEC in the framework of soft-collinear effective theory (SCET) [41–44] and perform the resummation to N^3LL accuracy.

In the past few decades, extensive studies of various dijet event shapes, such as thrust [45–49], heavy-jet mass [50, 51] as well as EEC, have been conducted at e^+e^- colliders, establishing a comprehensive formalism for dijet resummation and non-perturbative corrections. However, calculations for trijet event shapes are scarce [36, 37, 40, 52–57], and the study of the trijet

configuration as power correction to traditional event shapes using modern approaches has only recently begun [58–63]. The simplicity of coplanar EEEC and the existence of a non-perturbative definition for the energy correlator make this observable an ideal candidate for exploring both perturbative and non-perturbative QCD dynamics. At future lepton colliders, such as CEPC [64–66], ILC [67, 68] and FCC-ee [69], the increased number of multi-jet events will enable precise measurements of the coplanar EEEC, allowing the determination of both Standard Model parameters (including α_s) and the non-perturbative power corrections. Moreover, the formalism we develop for $e^+e^- \rightarrow \gamma^* \rightarrow$ trijet in this paper can be readily extended to other processes at the Large Hadron Collider (LHC). For example, our work has important implications for studying top quark decay, particularly given the recent interest in the potential of applying the EEEC to obtain precise top quark mass measurements [70–73]. As pointed out in Ref. [71, 74], the Jacobian peak of the EEEC in top decay corresponds to exactly its coplanar limit in the top rest frame. Resumming the coplanar logarithms would lead to more accurate theoretical predictions for the EEEC of top decay and potentially improve the precision of the top mass measurements.

The outline of this paper is as follows. In Sec. 2, we discuss the trijet coplanar kinematics and derive the factorization theorem for Eq. (1.4), focusing on the quark channel where the three jets are initiated by a quark, an antiquark, and a gluon. We also discuss all the ingredients needed for resummation to N³LL. In Sec. 3, we compute the resummed distribution for τ_p to N³LL and provide estimations for perturbative uncertainties. In Sec. 4, we consider the three-gluon jet case, whose contribution is $\mathcal{O}(\alpha_s^2)$ suppressed. In Sec. 5, we focus on the fully differential distribution in terms of $\{s, \phi_1, \phi_2\}$, and study the $s \rightarrow 1$ limit with ϕ_1, ϕ_2 fixed. In Sec. 6, we investigate the non-perturbative corrections using the Monte Carlo program **Pythia8**, and derive a relation of the τ_p -projected EEEC to D -parameter.

2 Factorization in the coplanar limit

In this section, we study the factorization theorem for the coplanar EEEC in the $\tau_p \rightarrow 0$ limit. For e^+e^- collisions, there are three partonic channels: (1). $e^+e^- \rightarrow \gamma^*/Z \rightarrow q\bar{q}g$; (2). “light-by-glue” process, $e^+e^- \rightarrow \gamma^* \rightarrow ggg$; (3). “Z-by-glue” process, $e^+e^- \rightarrow Z \rightarrow ggg$, as summarized in Ref. [75]. Our paper will focus on the γ^* -mediated processes, including the $q\bar{q}g$ channel (two quark jets and one gluon jet) and ggg channel (three gluon jets). However, the analysis below can be applied to the other channels as well as other trijet processes.

Similar to other trijet event shapes, the coplanar EEEC is expected to factorize into a hard function, three jet functions, and a soft function. Note that the hard function for the ggg channel only starts at two-loop order, which is $\mathcal{O}(\alpha_s^2)$ suppressed compared to the $q\bar{q}g$ channel. For convenience, below we will use the $q\bar{q}g$ channel to derive the factorization theorem and the resummed formula, noting that these expressions can be extended to the ggg channel by appropriate substitution of the corresponding ingredients.

2.1 Kinematics

Let us start by considering the partonic Born process $e^+e^- \rightarrow \gamma^* \rightarrow q(p_q)\bar{q}(p_{\bar{q}})g(p_g)$ where each of the final-state particles initiates a jet. We will use $J_{1,2,3}$ and $\{q, \bar{q}, g\}$ interchangeably when discuss the kinematics: $p_{J_1} = p_q$, $p_{J_2} = p_{\bar{q}}$ and $p_{J_3} = p_g$. The coplanar three-jet limit

defines a plane spanned by these three separated jets. Collinear splittings and soft emissions in the jets recoil the particles correlated by the EEEC observable slightly away from this plane. The kinematics of the factorization lies in a relation between the τ_p and the momentum perpendicular to the scattering plane, which we will denote as the y component, as illustrated in Fig. 2.

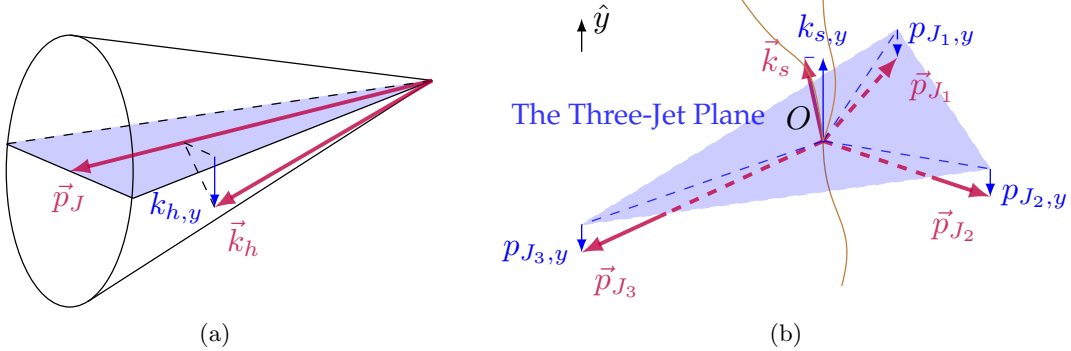


Figure 2: a) Collinear splitting within one jet. Hadron h slightly deviates from the momentum direction of the jet. b) The soft emissions accumulate to a total momentum \vec{k}_s , which results in a slight recoil of the three jets, pushing them slightly out of the trijet plane.

Now, consider three final-state hadrons with momenta k_{h_1} , k_{h_2} , and k_{h_3} , originating from jets J_1 , J_2 and J_3 respectively. In addition to the recoil effect of the total soft momentum $k_{s,y}$, they also obtain transverse momenta from the momentum components off the scattering plane due to final-state collinear splittings. Explicitly, the soft recoil contribution to $\tau_{h_1 h_2 h_3}$ is proportional to $k_{s,y}$ times the area of the triangle (the blue triangle in Fig. 2b) formed by the three jets, $|\vec{p}_{J_1} \times \vec{p}_{J_2}|$, and a normalization factor $1/(E_{J_1} E_{J_2} E_{J_3})$ which reflects the fact that $\tau_{h_1 h_2 h_3}$ in Eq. (1.3) is defined using the unit vectors. In the $\tau_p \rightarrow 0$ limit, we find the volume of parallelepiped to be

$$\tau_{h_1 h_2 h_3} = \frac{|\vec{p}_{J_1} \times \vec{p}_{J_2}|}{E_{J_1} E_{J_2} E_{J_3}} \left| \frac{k_{h_1,y}}{z_{h_1}} + \frac{k_{h_2,y}}{z_{h_2}} + \frac{k_{h_3,y}}{z_{h_3}} - k_{s,y} \right| + \text{power corrections ,} \quad (2.1)$$

where z_{h_1} is the longitudinal momentum ratio of k_{h_1} with respect to p_{J_1} , and similarly for z_{h_2} and z_{h_3} . Collinear splittings of hadron h deviated from the direction of \vec{p}_J , further adds a contribution of $k_{h,y}/z_h$.

For convenience, we define $\xi = \frac{|\vec{p}_{J_1} \times \vec{p}_{J_2}| Q}{E_{J_1} E_{J_2} E_{J_3}}$, which can be written in terms of jet energies

$$\begin{aligned} \xi &= \frac{|\vec{p}_{J_1} \times \vec{p}_{J_2}| Q}{E_{J_1} E_{J_2} E_{J_3}} \\ &= \frac{Q \sqrt{(E_{J_1} + E_{J_2} + E_{J_3})(E_{J_2} + E_{J_3} - E_{J_1})(E_{J_3} + E_{J_1} - E_{J_2})(E_{J_1} + E_{J_2} - E_{J_3})}}{2 E_{J_1} E_{J_2} E_{J_3}} \\ &= \frac{4\sqrt{uvw}}{(1-u)(1-v)(1-w)} . \end{aligned} \quad (2.2)$$

In the second line, we have used Heron's formula for the area of a triangle with sides E_{J_1} , E_{J_2} , E_{J_3} . In the third line, we introduce three dimensionless variables u , v and w via

$$u = \frac{s_{q\bar{q}}}{Q^2}, \quad v = \frac{s_{qg}}{Q^2}, \quad w = \frac{s_{\bar{q}g}}{Q^2}, \quad \text{with } s_{ij} = (p_i + p_j)^2, \quad (2.3)$$

satisfying $u + v + w = 1$ in the massless limit.

Putting everything together, at leading power, our measurement function takes the form of $\delta\left(\tau_p - \frac{\xi}{Q} \left| \frac{k_{h_1,y}}{z_{h_1}} + \frac{k_{h_2,y}}{z_{h_2}} + \frac{k_{h_3,y}}{z_{h_3}} - k_{s,y} \right| \right)$. Since the observable receives a contribution from perpendicular momenta, we will characterize the collinear splittings by the TMD fragmentation functions (TMDFFs) and the global soft emissions by a TMD trijet soft function. Now we are ready to write down the factorization theorem.

2.2 Factorization theorem

Given the kinematic analysis, the coplanar EEEC cross-section is factorized as

$$\begin{aligned} \frac{1}{\sigma_{\text{LO}}} \frac{d\sigma_q}{d\tau_p} &= \int_T dv dw H_q(v, w, \mu) \sum_{h_1, h_2, h_3} \int dk_{h_1, y} \int dk_{h_2, y} \int dk_{h_3, y} \int dz_{h_1} \int dz_{h_2} \int dz_{h_3} \\ &\times z_{h_1} z_{h_2} z_{h_3} F_{h_1/q}(k_{h_1, y}, z_{h_1}, \mu, \nu) F_{h_2/\bar{q}}(k_{h_2, y}, z_{h_2}, \mu, \nu) F_{h_3/g}(k_{h_3, y}, z_{h_3}, \mu, \nu) \\ &\times S_q(k_{s,y}, \mu, \nu) \delta\left(\tau_p - \xi \left| \frac{k_{h_1,y}}{z_{h_1}} + \frac{k_{h_2,y}}{z_{h_2}} + \frac{k_{h_3,y}}{z_{h_3}} - k_{s,y} \right| \right) + \text{power corrections}, \end{aligned} \quad (2.4)$$

where T is the domain of the dv and dw integral which is constrained by the phase-space cuts from the jet algorithm. For the case of $y_{\text{cut}} = 0.1$, T is plotted in Fig. 3. The subscript q on the LHS denotes the $\gamma^* \rightarrow q\bar{q}g$ channel. We also adopt the normalization

$$\sigma_{\text{LO}} = \frac{\alpha_s(Q)}{4\pi} C_F \sigma_0, \quad (2.5)$$

where σ_0 is the Born cross-section for $e^+e^- \rightarrow q\bar{q}$. This ensures that the order counting of the coplanar EEEC matches that of traditional dijet event shape resummation. H_q and S_q are the trijet hard function and the trijet TMD soft function respectively. The subscript q here denotes the quark channel. The hard function $H_q(v, w, \mu)$ is obtained by matching SCET to QCD. In fixed-order perturbation theory, it can be expanded as $H_q(v, w, \mu) = \sum_{n=0} \left(\frac{\alpha_s(\mu)}{4\pi}\right)^n H_q^{(n)}(v, w, \mu)$. The σ_{LO} normalization in Eq. (2.4) implies that the hard function is normalized such that its leading order begins at $\mathcal{O}(\alpha_s^0)$. The soft function S_q is defined as a vacuum expectation value of Wilson lines,

$$S_q(n_q, n_{\bar{q}}, n_g, b_y) = \text{tr} \langle 0 | T[\mathbf{S}_{n_q} \mathbf{S}_{n_{\bar{q}}} \mathbf{S}_{n_g}(0^\mu)] \bar{T}[\mathbf{S}_{n_q}^\dagger \mathbf{S}_{n_{\bar{q}}}^\dagger \mathbf{S}_{n_g}^\dagger(0^+, 0^-, 0_x, b_y)] | 0 \rangle, \quad (2.6)$$

where the soft Wilson line \mathbf{S}_{n_i} is defined as

$$\mathbf{S}_{n_i}(x) = \mathcal{P} \exp \left(ig_s \int_{-\infty}^0 ds n_i \cdot A_s(x + sn_i) \mathbf{T}_i \right). \quad (2.7)$$

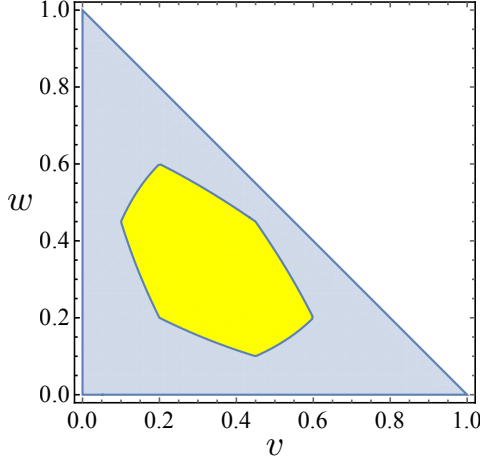


Figure 3: The phase space T for $y_3 > y_{\text{cut}}$ with $y_{\text{cut}} = 0.1$ is shown as the yellow region, plotted in v and w axes. The blue region is the total 3-body phase space.

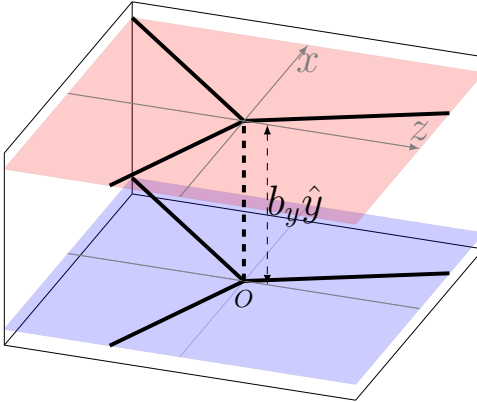


Figure 4: The spatial structure of the coplanar EEEC soft function. Each set of Wilson lines lies on the trijet plane, and their relative displacement is perpendicular to the plane.

Here b_y is the conjugate variable to $k_{s,y}$. We use the color space notation from Ref. [39] and the trace is over the color indices. Notice that the Wilson lines are in either fundamental or adjoint representation, depending on i being quark or gluon. The spatial structure of the Wilson lines is indicated in Fig. 4. Calculations of the soft function will be discussed in Sec. 2.3.3.

In addition, $F_{h/i}$ with $i = q, \bar{q}, g$ are the TMD fragmentation functions (TMDFFs), which describe the collinear radiation of a final-state hadron h from the splitting of the parton i , with energy fraction z_h and y component (perpendicular to the three-jet plane) of transverse momentum, $k_{h,y}$. $F_{h/f}$ here are the TMDFFs in the parton frame, by which we mean the frame where the parton has zero transverse momentum. However, it is usually easier to give an operator definition of the TMDFFs in the hadron frame, where hadron h has zero transverse momentum. We use D to denote the hadron-frame TMDFFs, defined in position space as [76]

$$D_{h/q}(\vec{b}_\perp, z_h) = \frac{1}{2z_h N_c} \sum_X \int \frac{db^+}{4\pi} e^{ik^- b^+ / (2z_h)} \text{tr}_{\text{spin}} \langle 0 | \frac{\not{b}}{2} \chi_n(b) | h, X \rangle \langle h, X | \bar{\chi}_n(0) | 0 \rangle, \quad (2.8)$$

$$D_{h/g}(\vec{b}_\perp, z_h) = -\frac{k_h^- g_{\perp\mu\nu}}{(d-2)(N_c^2-1)z_h^2} \sum_X \int \frac{db^+}{4\pi} e^{ik_h^- b^+/(2z_h)} \langle 0 | \mathcal{B}_{n\perp}^\mu(b) | h, X \rangle \langle h, X | \mathcal{B}_{n\perp}^\nu(0) | 0 \rangle. \quad (2.9)$$

where χ_n and \mathcal{B}_n^μ are in the SCET notation, denoting the gauge invariant n -collinear quark and gluon fields respectively. Note that in Eq. (2.9) we keep only the transverse polarization contribution of the gluon since the linear polarization does not contribute to the process considered here. The pair of fields are separated by a space-like distance $b^\mu = (b^+, 0^-, \vec{b}_\perp)$, where \vec{b}_\perp is the conjugate variable to the parton's transverse momentum relative to \vec{n} . A detailed discussion of the relation between the TMDFFs in the two frames can be found in Refs. [76–78]; Here we simply state the result,

$$F_{h/i}(\vec{b}_T/z_h, z_h) = z_h^{2-2\epsilon} D_{h/i}(\vec{b}_T, z_h). \quad (2.10)$$

The operator product expansion (OPE) of the TMDFF onto the standard fragmentation functions is given in momentum space by

$$F_{h/i}(\vec{k}_{h\perp}, z_h) = \sum_j \int \frac{dx_h}{x_h^3} d_{h/f}(x_h) \mathcal{J}_{fi} \left(\frac{\vec{k}_{h\perp}}{x_h}, \frac{z_h}{x_h} \right) + \text{power corrections}, \quad (2.11)$$

where \mathcal{J}_{fi} are finite matching coefficients, and $d_{h/f}$ are the fragmentation functions. To convert these TMDFFs as well as their matching coefficients to the ones shown in Eq. (2.4) as functions of the y -component momenta, one simply integrates out their x components,

$$F_{h/i}(k_{h,y}, z_h) = \int dk_{h,x} F_{h/i}(\vec{k}_{h\perp}, z_h), \quad \text{and} \quad \mathcal{J}_{fi}(k_y, \xi) = \int dk_x \mathcal{J}_{fi}(\vec{k}_\perp, \xi), \quad (2.12)$$

so that we have

$$F_{h/i}(k_{h,y}, z_h) = \sum_f \int \frac{dx_h}{x_h^2} d_{h/f}(x_h) \mathcal{J}_{fi} \left(\frac{k_{h,y}}{x_h}, \frac{z_h}{x_h} \right) + \text{power corrections}. \quad (2.13)$$

Now let us plug the above equation into the factorization formula (2.4) and simplify the result on the right-hand side. Explicitly, we insert Eq. (2.13) into Eq. (2.4), and change the variables from $\{z_{h_1}, x_{h_1}\}$ to $\{\zeta_{f_1}, x_{h_1}\}$

$$\zeta_{f_1} = \frac{z_{h_1}}{x_{h_1}}, \quad dz_{h_1} dx_{h_1} = x_{h_1} d\zeta_{f_1} dx_{h_1}, \quad (2.14)$$

and similarly from $\{z_{h_2}, x_{f_2}\}$ to $\{\zeta_{f_2}, x_{h_2}\}$ and from $\{z_{h_3}, x_{h_3}\}$ to $\{\zeta_{f_3}, x_{h_3}\}$. We then find

$$\begin{aligned} \frac{1}{\sigma_{\text{LO}}} \frac{d\sigma_q}{d\tau_p} &= \int_D dv dw H_q(v, w, \mu) \sum_{f_1, f_2, f_3} \int dk_{f_1, y} \int dk_{f_2, y} \int dk_{f_3, y} \int dk_{s, y} \int d\zeta_{f_1} \int d\zeta_{f_2} \int d\zeta_{f_3} \zeta_{f_1} \zeta_{f_2} \zeta_{f_3} \\ &\times S(k_{s, y}, \mu, \nu) \delta \left(\tau_p - \xi \left| \frac{k_{f_1, y}}{\zeta_{f_1}} + \frac{k_{f_2, y}}{\zeta_{f_2}} + \frac{k_{f_3, y}}{\zeta_{f_3}} - k_{s, y} \right| \right) \left[\sum_{h_1} \int dx_{h_1} x_{h_1} d_{h_1/f_1}(x_{h_1}, \mu) \right] \mathcal{J}_{f_1 q}(k_{f_1, y}, \zeta_{f_1}) \\ &\times \left[\sum_{h_2} \int dx_{h_2} x_{h_2} d_{h_2/f_2}(x_{h_2}, \mu) \right] \mathcal{J}_{f_2 \bar{q}}(k_{f_2, y}, \zeta_{f_2}) \left[\sum_{h_3} \int dx_{h_3} x_{h_3} d_{h_3/f_3}(x_{h_3}, \mu) \right] \mathcal{J}_{f_3 g}(k_{f_3, y}, \zeta_{f_3}) \end{aligned}$$

+ power corrections , (2.15)

with $k_{f_1,y} = \frac{k_{h_1,y}}{x_{h_1}}$, $k_{f_2,y} = \frac{k_{h_2,y}}{x_{h_2}}$, $k_{f_3,y} = \frac{k_{h_3,y}}{x_{h_3}}$. The integrals inside the square brackets are simply unity due to the momentum-conservation sum rule

$$\sum_h \int dx \ x \ d_{h/i}(x) = 1. \quad (2.16)$$

To further simplify the factorization formula, we define the position-space matching coefficients and the soft function

$$\mathcal{J}_{fi}(b_y) = \int dk_y e^{ib_y k_y} \mathcal{J}_{fi}(k_y, \zeta), \quad (2.17)$$

$$S(b_y) = \int dk_{s,y} e^{ib_y k_{s,y}} S(k_{s,y}), \quad (2.18)$$

as well as the jet function

$$J_i(b_y) = \sum_f \int_0^1 d\zeta \ \zeta \ \mathcal{J}_{fi}\left(\frac{b_y}{\zeta}, \zeta\right), \quad i, f \in \{q, \bar{q}, g\}, \quad (2.19)$$

and apply the Fourier representation of the measurement function

$$\begin{aligned} \delta \left(\tau_p - \xi \left| \frac{k_{f_1,y}}{\zeta_{f_1}} + \frac{k_{f_2,y}}{\zeta_{f_2}} + \frac{k_{f_3,y}}{\zeta_{f_3}} - k_{s,y} \right| \right) &= \int_{-\infty}^{\infty} \frac{db_y}{2\pi\xi} 2 \cos(b_y \tau_p / \xi) \\ &\times \exp \left[ib_y \left(\frac{k_{f_1,y}}{\zeta_{f_1}} + \frac{k_{f_2,y}}{\zeta_{f_2}} + \frac{k_{f_3,y}}{\zeta_{f_3}} - k_{s,y} \right) \right]. \end{aligned} \quad (2.20)$$

Then we arrive at the final factorization formula for the EEEC in the coplanar limit

$$\begin{aligned} \frac{1}{\sigma_{\text{LO}}} \frac{d\sigma_q}{d\tau_p} &= \int_T dv dw H_q(v, w, \mu) \int_{-\infty}^{\infty} \frac{db_y}{2\pi\xi} 2 \cos \left(\frac{b_y \tau_p}{\xi} \right) S(b_y, \mu, \nu) J_q(b_y, \mu, \nu) J_{\bar{q}}(b_y, \mu, \nu) J_g(b_y, \mu, \nu) \\ &+ \text{power corrections}. \end{aligned} \quad (2.21)$$

2.3 Ingredients

In this subsection, we will discuss all the ingredients appearing in the final factorized formula (2.21), as well as the UV and rapidity renormalization group equations (RGEs) they satisfy. In particular, we will see that up to two-loop accuracy, our trijet soft function factorizes into a product of three dipole TMD soft functions, which are known to three loops analytically [79, 80]. The simplicity of the soft function is one main reason that allows us to reach the N³LL accuracy for the coplanar EEEC.

2.3.1 Hard Function

The hard function can be obtained by matching the QCD current into the corresponding SCET current operator. At leading order, the hard function is simply proportional to the tree-level process $e^+e^- \rightarrow q\bar{q}g$:

$$H_q^{(0)}(v, w, \mu) = 2 \frac{(1-v)^2 + (1-w)^2}{vw}, \quad (2.22)$$

where subscript q denotes the quark channel. At NLO and beyond, since all virtual graphs in SCET are scaleless in dimensional regularization, we can extract the trijet hard function from the virtual contribution in squared QCD matrix elements $e^+e^- \rightarrow 3$ partons. Such a hard function is the same as direct photon production or 3-jetness by crossing. We begin our extraction of the hard function at NNLO accuracy by examining the form factor results for $e^+e^- \rightarrow q\bar{q}g$ up to NNLO [81–83]. For our purposes, we utilize the UV-renormalized and IR-unsubtracted results from the decay region as presented in Ref. [83]. It is worth noting that the results in Ref. [83] are presented with $\mu^2 = Q^2$. Given that scale dependence can arise from both UV and IR origins, we opt to reconstruct the scale by first outlining a general form for the UV-unrenormalized and IR-unsubtracted form factors:

$$\langle \mathcal{M}_{q\bar{q}g}^{\text{bare}} \rangle = g_s^{\text{bare}} \left\{ \langle \mathcal{M}_{q\bar{q}g}^{(0)} \rangle + \frac{\alpha_s^{\text{bare}}}{4\pi} \left(\frac{Q^2}{\mu^2} \right)^{-\epsilon} \langle \mathcal{M}_{q\bar{q}g}^{(1)} \rangle + \left(\frac{\alpha_s^{\text{bare}}}{4\pi} \right)^2 \left(\frac{Q^2}{\mu^2} \right)^{-2\epsilon} \langle \mathcal{M}_{q\bar{q}g}^{(2)} \rangle + \mathcal{O}(\alpha_s^3) \right\}. \quad (2.23)$$

It is important to observe that $\langle \mathcal{M}_{q\bar{q}g}^{(i)} \rangle$ for $i = 0, 1, 2$ are independent of the scale μ ; all scale dependence is derived from the prefactor $\left(\frac{Q^2}{\mu^2} \right)^{-\epsilon}$. Following this, we conduct the strong coupling renormalization by implementing these substitutions:

$$\alpha_s^{\text{bare}} \rightarrow \alpha_s Z_{\alpha_s}, \quad g_s^{\text{bare}} = g_s \sqrt{Z_{\alpha_s}},$$

where

$$Z_{\alpha_s} = 1 - \frac{\beta_0}{\epsilon} \frac{\alpha_s}{4\pi} - \left(\frac{\beta_0^2}{\epsilon^2} - \frac{\beta_1}{2\epsilon} \right) \left(\frac{\alpha_s}{4\pi} \right)^2 + \mathcal{O}(\alpha_s^3), \quad (2.24)$$

Here, β_i represents the QCD beta function, which can be found in App. A. This UV renormalization procedure yields UV-finite results, allowing us to determine $\langle \mathcal{M}_{q\bar{q}g}^{(i)} \rangle$ for $i = 0, 1, 2$ by comparing our results with those in Ref. [83]. This method enables us to recover the scale dependence for the form factor. Next, we address the IR subtraction for the UV-finite form factors. The IR singularities of massless scattering amplitudes are well-understood [84–87] and are governed by a multiplicative renormalization factor \mathbf{Z} . In our context, this relationship is expressed as:

$$\langle \mathcal{M}^{\text{finite}} q\bar{q}g \rangle = \mathbf{Z}^{-1} \langle \mathcal{M} q\bar{q}g \rangle, \quad (2.25)$$

In this equation, $\langle \mathcal{M} q\bar{q}g \rangle$ represents the UV-renormalized but IR-unsubtracted amplitude, while \mathbf{Z}^{-1} serves to minimally subtract the IR divergences in $\langle \mathcal{M} q\bar{q}g \rangle$, ensuring that the left-hand side of the equation remains finite. Finally, we extract the hard function with proper normalization:

$$H_q(v, w, \mu) = \frac{1}{C_F \alpha_s / (4\pi)} \langle \mathcal{M}^{\text{finite}} q\bar{q}g | \mathcal{M}^{\text{finite}} q\bar{q}g \rangle. \quad (2.26)$$

In the ancillary file, we provide the expressions for the hard function up to two loops.

The extracted hard function satisfies the following RG equation,

$$\frac{d \ln H_q(v, w, \mu)}{d \ln \mu^2} = -\gamma_{\text{cusp}}(\alpha_s) \sum_{1 \leq i < j \leq 3} \mathbf{T}_i \cdot \mathbf{T}_j \ln \frac{s_{ij}}{\mu^2} + \sum_{i=1}^3 \gamma_i(\alpha_s) \quad (2.27)$$

$$+ \gamma_{\text{quad}}(\alpha_s) f_{abe} f_{cde} \sum_{i=1}^3 \sum_{\substack{1 \leq j < k \leq 3 \\ j, k \neq i}} \{\mathbf{T}_i^a, \mathbf{T}_i^d\} \mathbf{T}_j^b \mathbf{T}_k^c + \mathcal{O}(\alpha_s^4),$$

where \mathbf{T}_i 's are Catani-Seymour's color insertion operator [39]. The $\mathbf{T}_i \cdot \mathbf{T}_j$ term in Eq. (2.27) is the dipole contribution. The second line is the quadrupole color contribution (involving four color operators) which starts at three loops and was calculated in Refs. [88, 89], which is a constant without any kinematic dependence,³

$$\gamma_{\text{quad}} = \left(\frac{\alpha_s}{4\pi}\right)^3 16 (\zeta_5 + 2\zeta_2 \zeta_3) + \mathcal{O}(\alpha_s^4). \quad (2.28)$$

For the $q\bar{q}g$ color singlet state, we can replace $\mathbf{T}_i \cdot \mathbf{T}_j$ in Eq. (2.27) with the Casimir factors by making use of the overall color conservation $\mathbf{T}_q + \mathbf{T}_{\bar{q}} + \mathbf{T}_g = 0$,

$$\mathbf{T}_q \cdot \mathbf{T}_g = \frac{1}{2}(\mathbf{T}_{\bar{q}}^2 - \mathbf{T}_q^2 - \mathbf{T}_g^2) = -\frac{C_A}{2}, \quad (2.29a)$$

$$\mathbf{T}_{\bar{q}} \cdot \mathbf{T}_g = \frac{1}{2}(\mathbf{T}_q^2 - \mathbf{T}_{\bar{q}}^2 - \mathbf{T}_g^2) = -\frac{C_A}{2}, \quad (2.29b)$$

$$\mathbf{T}_q \cdot \mathbf{T}_{\bar{q}} = \frac{1}{2}(\mathbf{T}_g^2 - \mathbf{T}_q^2 - \mathbf{T}_{\bar{q}}^2) = \frac{C_A - 2C_F}{2}. \quad (2.29c)$$

And the color quadrupole color factor can be calculated to be

$$f_{abe} f_{cde} \sum_{i=1}^3 \sum_{\substack{1 \leq j < k \leq 3 \\ j, k \neq i}} \{\mathbf{T}_i^a, \mathbf{T}_i^d\} \mathbf{T}_j^b \mathbf{T}_k^c |q\bar{q}g\rangle = |q\bar{q}g\rangle \frac{3}{2} C_A, \quad (2.30)$$

by noticing that the color state $|q^\alpha \bar{q}^\beta g^a\rangle$ has only one color structure which is proportional to $T_{\alpha\beta}^a$, where α, β, a are color indices for q, \bar{q}, g respectively.

It is convenient to absorb the kinematic dependence in the cusp piece into the non-cusp piece. This leads to the final RGE for the hard function

$$\frac{d \ln H_q(v, w, \mu)}{d \ln \mu^2} = \frac{C_A + 2C_F}{2} \gamma_{\text{cusp}}(\alpha_s) \ln \frac{Q^2}{\mu^2} + \gamma_{h,q}(v, w, \alpha_s), \quad (2.31)$$

where we define the non-cusp piece to be

$$\begin{aligned} \gamma_{h,q}(v, w, \alpha_s) &= \gamma_{\text{cusp}}(\alpha_s) \left(\frac{C_A}{2} \ln v + \frac{C_A}{2} \ln w + \frac{2C_F - C_A}{2} \ln(1 - v - w) \right) \\ &\quad + 2\gamma_q(\alpha_s) + \gamma_g(\alpha_s) + \frac{3}{2} C_A \gamma_{\text{quad}}[\alpha_s]. \end{aligned} \quad (2.32)$$

The solution to the RG equation is formally given by

$$H_q(v, w, \mu) = H_q(v, w, \mu_h) \exp \left[\int_{\mu_h^2}^{\mu^2} \frac{d\bar{\mu}^2}{\bar{\mu}^2} \left(\frac{C_A + 2C_F}{2} \gamma_{\text{cusp}}(\alpha_s(\bar{\mu})) \ln \frac{Q^2}{\bar{\mu}^2} + \gamma_{h,q}(v, w, \alpha_s(\bar{\mu})) \right) \right]. \quad (2.33)$$

³For processes that involve four or more partons, the quadrupole contribution includes terms involving four lightlike directions and has nontrivial dependence on kinematics. The nontrivial kinematic dependence comes through a cross ratio of four lightlike vectors. For the case here, the quadrupole contribution is a constant since it is impossible to construct a nontrivial scaling invariant from three lightlike vectors.

For convenience, we define the following RG notations:

$$\begin{aligned} S_\Gamma(\nu, \mu) &= - \int_{\alpha_s(\nu)}^{\alpha_s(\mu)} d\alpha \frac{\gamma_{\text{cusp}}(\alpha)}{\beta(\alpha)} \int_{\alpha_s(\nu)}^\alpha \frac{d\alpha'}{\beta(\alpha')}, \\ A_\Gamma(\nu, \mu) &= - \int_{\alpha_s(\nu)}^{\alpha_s(\mu)} d\alpha \frac{\gamma_{\text{cusp}}(\alpha)}{\beta(\alpha)}, \\ A_{\gamma_j}(\nu, \mu) &= - \int_{\alpha_s(\nu)}^{\alpha_s(\mu)} d\alpha \frac{\gamma_j(\alpha)}{\beta(\alpha)}, \end{aligned} \quad (2.34)$$

Then Eq. (2.33) can be rewritten as

$$H_q(v, w, \mu) = H_q(v, w, \mu_h) \exp [2(C_A + 2C_F)S_\Gamma(\mu_h, \mu) - 2A_{\gamma_{h,q}}(\mu_h, \mu)] \left(\frac{Q^2}{\mu_h^2} \right)^{-(C_A + 2C_F)A_\Gamma(\mu_h, \mu)}. \quad (2.35)$$

The explicit expressions of the running coupling and these RG kernels are given in App. A.

2.3.2 Jet function

The jet functions needed for the coplanar EEEC defined in Eq. (2.20) are the same as the jet functions in both the back-to-back limit of the EEC [23] and the TEEC [28, 29]. The fixed-order calculation has been pushed to N³LO [90, 91], and we quote the one-loop result for illustration,

$$\begin{aligned} J_q(b_y, \mu, \nu) &= J_{\bar{q}}(b_y, \mu, \nu) = 1 + \left(\frac{\alpha_s}{4\pi} \right) (-2C_F L_b L_\omega + 3C_F L_b + c_q^1) + \mathcal{O}(\alpha_s^2), \\ J_g(b_y, \mu, \nu) &= 1 + \left(\frac{\alpha_s}{4\pi} \right) [-2C_A L_b L_\omega + \beta_0 L_b + c_g^1] + \mathcal{O}(\alpha_s^2). \end{aligned} \quad (2.36)$$

Here $L_b = \ln(b_y^2 \mu^2 / b_0^2)$ and $L_\omega = \ln \omega^2 / \nu^2$, where $\omega = \bar{n}_i \cdot p_i$ is the large momentum of the jet i (\bar{n}_i here is the auxiliary lightcone vector opposite to the n_i direction satisfying $n_i \cdot \bar{n}_i = 2$). Explicitly, for the three jets p_q , $p_{\bar{q}}$ and p_g , we have

$$\omega_q = Q(1 - w), \quad \omega_{\bar{q}} = Q(1 - v), \quad \omega_g = Q(v + w). \quad (2.37)$$

The one-loop jet constants are

$$c_q^1 = C_F(4 - 8\zeta_2), \quad c_g^1 = \left(\frac{65}{18} - 8\zeta_2 \right) C_A - \frac{5}{18} n_f. \quad (2.38)$$

The jet functions satisfy the following UV and RG equations,

$$\frac{d \ln J_i}{d \ln \mu^2} = -\frac{1}{2} c_i \gamma_{\text{cusp}} \ln \frac{\omega_i^2}{\nu^2} + \gamma_{J,i}, \quad (2.39)$$

$$\frac{d \ln J_i}{d \ln \nu^2} = \frac{1}{2} c_i \left(\int_{b_0^2/b_y^2}^{\mu^2} \frac{d\bar{\mu}^2}{\bar{\mu}^2} \gamma_{\text{cusp}}[\alpha_s(\bar{\mu})] - \gamma_r[\alpha_s(b_0/b_y)] \right). \quad (2.40)$$

with $i = q, g$ for quark/gluon jet function, $\gamma_{J,i}$ the jet anomalous dimensions and γ_r the rapidity anomalous dimension. These results are summarized in App. B. Solving these equations gives the following solution,

$$J_i(\mu, \nu) = J_i(\mu_j, \nu_j) \left(\frac{\nu^2}{\nu_j^2} \right)^{-c_i A_\Gamma\left(\frac{b_0}{b_y}, \mu_j\right) - \frac{1}{2} c_i \gamma_r \left[\alpha_s\left(\frac{b_0}{b_y}\right) \right]} \left(\frac{\omega_i^2}{\nu^2} \right)^{c_i A_\Gamma(\mu_j, \mu)} e^{-2A_{\gamma_{J,i}}(\mu_j, \mu)}. \quad (2.41)$$

2.3.3 Soft Function

The trijet soft function in the coplanar EEEC is the same as the TEEC soft function with three Wilson lines [28, 29] (detailed discussion for it can be found in Ref. [29]). For the purpose of this paper, to achieve the N³LL accuracy, we need the two-loop constants and the three-loop anomalous dimensions. Thanks to the non-abelian exponentiation theorem [92, 93], the soft function can be written as the exponential of web diagrams. Up to two loops, this soft function has only dipole contributions,⁴

$$S_q = \exp \left[- \sum_{1 \leq i < j \leq 3} \mathbf{T}_i \cdot \mathbf{T}_j S_{ij} + \mathcal{O}(\alpha_s^3) \right]. \quad (2.42)$$

where we have used the notation $\{1, 2, 3\}$ and $\{q, \bar{q}, g\}$ interchangeably, and S_{ij} is the dipole contribution with lightcone directions n_i and n_j . S_{ij} here can be simply written as

$$S_{ij} = S_\perp \left(L_b, L_\nu + \ln \frac{n_i \cdot n_j}{2} \right), \quad (2.43)$$

where $L_\nu = \ln \nu^2 b_y^2 / b_0^2$, and $S_\perp(L_b, L_\nu)$ is the TMD soft function for color singlet production at hadron colliders (defined as the vacuum matrix element of back-to-back soft Wilson lines), which can be found up to three loops in [79]. In other words, going from the back-to-back dipole soft function to general n_i, n_j lightcone directions, amounts to shift the rapidity logarithm L_ν by a boost factor $\ln(n_i \cdot n_j)/2$.

Starting from three loops, there are also contributions involving three Wilson lines, and it would be interesting to calculate them using the soft current in [94]. The scale-dependent part of this three-Wilson-line contribution can be predicted by the quadrupole term in Eq. (2.44) below, while the scale-independent part is beyond the working order of this paper.

The RG equations for the soft function are

$$\begin{aligned} \frac{d \ln S_q(n_q, n_{\bar{q}}, n_g, b_y, \mu, \nu)}{d \ln \mu^2} = & - \sum_{1 \leq i < j \leq 3} \mathbf{T}_i \cdot \mathbf{T}_j \left(\gamma_{\text{cusp}}(\alpha_s) \ln \frac{\mu^2}{\nu^2 (n_i \cdot n_j)/2} - \gamma_s(\alpha_s) \right) \\ & - f_{abe} f_{cde} \sum_{i=1}^3 \sum_{\substack{1 \leq j < k \leq 3 \\ j, k \neq i}} \{ \mathbf{T}_i^a, \mathbf{T}_i^d \} \mathbf{T}_j^b \mathbf{T}_k^c \gamma_{\text{quad}}(\alpha_s) + \mathcal{O}(\alpha_s^4), \end{aligned} \quad (2.44)$$

$$\frac{d \ln S_q(n_q, n_{\bar{q}}, n_g, b_y, \mu, \nu)}{d \ln \nu^2} = - \sum_{1 \leq i < j \leq 3} \mathbf{T}_i \cdot \mathbf{T}_j \left(\int_{\mu^2}^{b_0^2/b_y^2} \frac{d\bar{\mu}^2}{\bar{\mu}^2} \gamma_{\text{cusp}}(\alpha_s[\bar{\mu}]) + \gamma_r(\alpha_s[b_0/b_y]) \right). \quad (2.45)$$

The first line in Eq. (2.44) is the dipole contribution and the second line is the quadrupole contribution. Similar structure also appeared for the hard function in Eq. (2.27). As discussed in the hard function section, note that γ_{quad} does not have kinematic dependence on v and w , since it is impossible to construct a scaling invariant from three light-like vectors.

⁴For the case of four-Wilson-line TEEC soft function, there is a tripole contribution (involving three Wilson lines) at two loops which is purely imaginary. As shown in Ref. [29], such contribution vanishes for the three-Wilson-line soft function here due to color conservation and antisymmetry of f^{abc} .

Similar to Sec. 2.3.1, here we can also replace $\mathbf{T}_i \cdot \mathbf{T}_j$ in Eqs. (2.44) and (2.45) by the overall Casimir factors using Eq. (2.29), and replace the quadrupole color factor with $\frac{3}{2}C_A$ using Eq. (2.30). We then write $n_i \cdot n_j$ in terms of kinematic variables v and w ,

$$\frac{n_q \cdot n_{\bar{q}}}{2} = \frac{(1-v-w)}{(1-v)(1-w)}, \quad \frac{n_q \cdot n_g}{2} = \frac{v}{(v+w)(1-w)}, \quad \frac{n_{\bar{q}} \cdot n_g}{2} = \frac{w}{(1-v)(v+w)}. \quad (2.46)$$

This leads to the final RG equations for the trijet soft function

$$\begin{aligned} \frac{d \ln S_q}{d \ln \mu^2} &= \left[\frac{2C_F + C_A}{2} \left(\gamma_{\text{cusp}}[\alpha_s] \ln \frac{\mu^2}{\nu^2} - \gamma_s[\alpha_s] \right) + C_F \gamma_{\text{cusp}}[\alpha_s] \ln \frac{(1-v)(1-w)}{1-v-w} \right. \\ &\quad \left. + \frac{C_A}{2} \gamma_{\text{cusp}}[\alpha_s] \ln \frac{(v+w)^2(1-v-w)}{vw} - \frac{3}{2} C_A \gamma_{\text{quad}}[\alpha_s] \right], \end{aligned} \quad (2.47)$$

$$\frac{d \ln S_q}{d \ln \nu^2} = \frac{2C_F + C_A}{2} \left(\int_{\mu^2}^{b_0^2/b_y^2} \frac{d\bar{\mu}^2}{\bar{\mu}^2} \gamma_{\text{cusp}}(\alpha_s[\bar{\mu}]) + \gamma_r(\alpha_s[b_0/b_y]) \right). \quad (2.48)$$

A solution is then given by

$$\begin{aligned} S_q(\mu, \nu) &= S_q(\mu_s, \nu_s) \left(\frac{\nu^2}{\nu_s^2} \right)^{-(2C_F+C_A)A_\Gamma(\mu_s, b_0/b_y) + \frac{2C_F+C_A}{2}\gamma_r(\alpha_s(b_0/b_y))} \left(\frac{\mu_s^2}{\nu^2} \right)^{-(2C_F+C_A)A_\Gamma(\mu_s, \mu)} \\ &\times \exp [-2(2C_F+C_A)S_\Gamma(\mu_s, \mu) + (2C_F+C_A)A_{\gamma_s}(\mu_s, \mu) + 3C_A A_{\gamma_{\text{quad}}}(\mu_s, \mu)] \\ &\times \exp \left[-2C_F \ln \frac{(1-v)(1-w)}{1-v-w} A_\Gamma(\mu_s, \mu) - C_A \ln \frac{(v+w)^2(1-v-w)}{vw} A_\Gamma(\mu_s, \mu) \right]. \end{aligned} \quad (2.49)$$

2.4 Resummed formula

Putting everything together in Eq. (2.21), we obtain the resummed expression for the coplanar EEEC. Using the following identities

$$\begin{aligned} S_\Gamma(\mu_1, \mu_2) + S_\Gamma(\mu_2, \mu_3) &= S_\Gamma(\mu_1, \mu_3) + \ln \frac{\mu_1}{\mu_2} A_\Gamma(\mu_2, \mu_3), \\ A_\Gamma(\mu_1, \mu_2) + A_\Gamma(\mu_2, \mu_3) &= A_\Gamma(\mu_1, \mu_3), \end{aligned} \quad (2.50)$$

and the relations between anomalous dimensions

$$2\gamma_{h,q} + 4\gamma_{J,q} + 2\gamma_{J,g} - (2C_F + C_A)\gamma_s - 3C_A\gamma_{\text{quad}} - \ln(1-v-w)(2C_F - C_A)\gamma_{\text{cusp}} - \ln(vw)C_A\gamma_{\text{cusp}} = 0, \quad (2.51)$$

we can simplify it into the following form:

$$\begin{aligned} \frac{1}{\sigma_{\text{LO}}} \frac{d\sigma_q}{d\tau_p} &= \int_T dv dw H_q(v, w, \mu_h) \int_{-\infty}^{\infty} \frac{db_y}{2\pi\xi} 2 \cos \left(\frac{b_y \tau_p}{\xi} \right) \\ &\times S_q(\mu_s, \nu_s) J_q(\mu_j, \nu_j) J_{\bar{q}}(\mu_j, \nu_j) J_g(\mu_j, \nu_j) \times W_q(\mu_h, \mu_s, \nu_s, \mu_j, \nu_j), \end{aligned} \quad (2.52)$$

with the RG kernel

$$\begin{aligned} W_q(\mu_h, \mu_s, \nu_s, \mu_j, \nu_j) &= \exp [2(2C_F + C_A)(S_\Gamma(\mu_h, \mu_j) - S_\Gamma(\mu_s, \mu_j))] \\ &\times \exp [-2A_{\gamma_{h,q}}(\mu_h, \mu_s) + 2A_{\gamma_{J,q}}(\mu_s, \mu_j) + 2A_{\gamma_{J,q}}(\mu_s, \mu_j) + 2A_{\gamma_{J,g}}(\mu_s, \mu_j)] \end{aligned}$$

$$\begin{aligned}
& \times \left(\frac{Q^2}{\mu_h^2} \right)^{(2C_F+C_A)A_\Gamma(\mu_j, \mu_h)} \times \left(\frac{\nu_j^2}{\nu_s^2} \right)^{\frac{2C_F+C_A}{2}\gamma_r[\alpha_s(b_0/b_y)] - (2C_F+C_A)A_\Gamma(\mu_j, b_0/b_y)} \\
& \times \left(\frac{\mu_s^2}{\nu_s^2} \right)^{(2C_F+C_A)A_\Gamma(\mu_j, \mu_s)} \times [(1-w)(1-v)]^{2C_F A_\Gamma(\mu_j, \mu_s)} (v+w)^{2C_A A_\Gamma(\mu_j, \mu_s)}. \tag{2.53}
\end{aligned}$$

In the simplified resummed formula, we eliminate the μ dependence, which means that the resummation is explicitly RG invariant. When including the $\mathcal{O}(\alpha_s^2)$ terms in the boundaries and expanding the resummed formula to $\mathcal{O}(\alpha_s^2)$, we explicitly verified that all the μ_h , μ_j , μ_s , ν_j and ν_s dependence is cancelled. This provides another nontrivial check on the RG consistency. Note that the modification from quadrupole contribution now sits in the hard anomalous dimension. With every ingredient at hand, we are ready to discuss the scale setting and perform the numerical Fourier integration.

3 N^3LL resummation

3.1 Fixed-order expansion

Before performing the numerical resummation, we need to verify the factorization theorem with the fixed-order data. Note that to eliminate the large logarithms in the hard, jet, and soft functions, we identify the following canonical scales (also illustrated in Fig. 5)

$$\mu_h = Q, \quad \mu_j = \frac{b_0}{b_y}, \quad \mu_s = \frac{b_0}{b_y}, \quad \nu_j = Q, \quad \nu_s = \frac{b_0}{b_y}. \tag{3.1}$$

Plugging to the resummed expression in Eq. (2.52), expanding in terms of α_s and performing

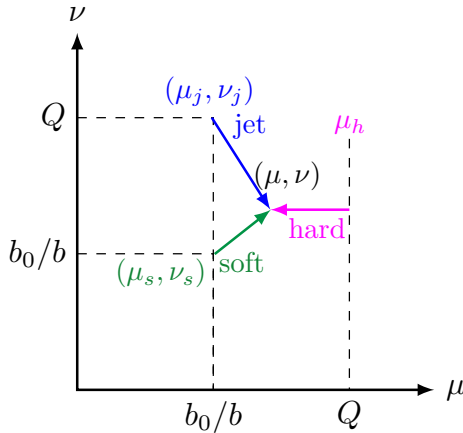


Figure 5: Illustration of all canonical scales and the running. The three modes (hard, jet, soft) live at different canonical renormalization and the rapidity scales, while the hard mode does not have a rapidity scale. One runs the RG evolutions and rapidity RG evolutions for the three modes to a common arbitrary scale (μ, ν) . The final result should not depend on (μ, ν) , as required by the RG consistency.

the inverse Fourier transformation, we find at $\mathcal{O}(\alpha_s)$

$$\begin{aligned} \frac{1}{\sigma_{\text{LO}}} \frac{d\sigma_q}{d\tau_p} = & \left(\frac{\alpha_s}{4\pi} \right) \int_T dv dw \left(\frac{v^2 - 2v + w^2 - 2w + 2}{vw} \right) \left\{ -16(C_A + 2C_F) \frac{\ln\left(\frac{2\tau_p}{\xi Q}\right)}{\tau_p} \right. \\ & + \left(8C_A \ln\left(\frac{vw}{1-v-w}\right) - \frac{44C_A}{3} + 16C_F \ln(1-v-w) - 24C_F + \frac{16T_F n_F}{3} \right) \frac{1}{\tau_p} \Big\} \\ & + \mathcal{O}(\alpha_s^2), \end{aligned} \quad (3.2)$$

where the v, w integrals can be performed numerically. To calculate the Fourier integrals analytically, we use the transformation rules between logarithms in Fourier space and plus distributions in the momentum space, summarized in App. C. The order α_s^2 expansion is rather long and we provide it in App. D. To crosscheck the double and single logarithms, we compare this expansion result with both LO and NLO distributions calculated using `NLOJet++` [40]. The comparison shows good agreements, see Fig. 6.

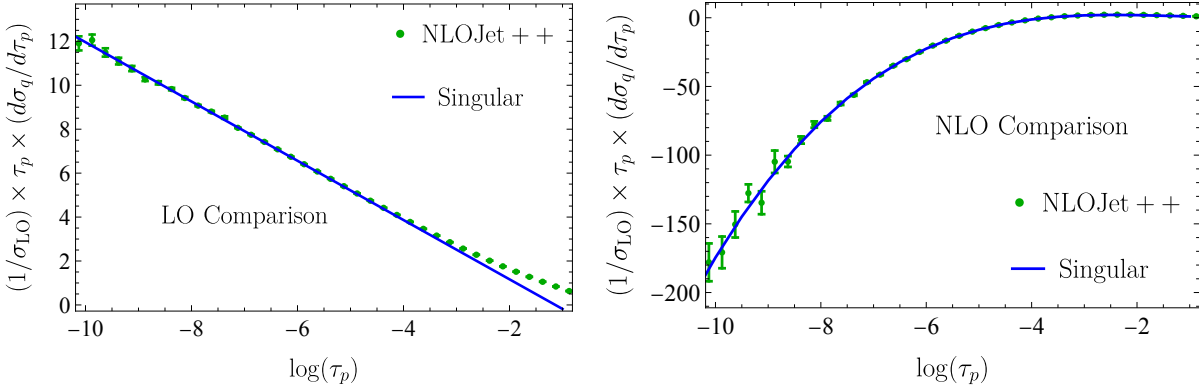


Figure 6: Comparison of the fixed-order expansion of the factorization formula (denoted as “singular” in the plots), with the numerical calculations using `NLOJet++` where two trillion events are sampled. We see perfect agreement between the two in the $\tau_p \rightarrow 0$ limit, and the error bars show the Monte Carlo errors from `NLOJet++`.

3.2 Resummation

To perform the resummation, we need to freeze the lowest scales to avoid the Landau pole. So instead of Eq. (3.2), we use the following canonical scale for numerical setup,

$$\mu_h^{\text{can}} = Q, \quad \mu_j^{\text{can}} = \sqrt{\frac{b_0^2}{b_y^2} + \frac{b_0^2}{b_{\max}^2}}, \quad \mu_s^{\text{can}} = \sqrt{\frac{b_0^2}{b_y^2} + \frac{b_0^2}{b_{\max}^2}}, \quad \nu_j^{\text{can}} = Q, \quad \nu_s^{\text{can}} = \sqrt{\frac{b_0^2}{b_y^2} + \frac{b_0^2}{b_{\max}^2}}, \quad (3.3)$$

where $b_0 = 2e^{-\gamma_E}$ and $b_{\max} = 1 \text{ GeV}^{-1}$. This prescription takes the jet, soft and rapidity soft scales to $\frac{b_0}{b_{\max}}$ when $b_y \rightarrow \infty$. We also do the same treatment for the $\gamma_r [\alpha_s(b_0/b_y)]$ in the RG kernel in Eq. (2.53).

Then we need to perform three numerical integrals as shown in Eq. (2.52). For the u, v integrals, we use the Monte Carlo integrator implemented in `Cuba` [95]. Note that the y_3 resolution

has cut off the region where $v \rightarrow 0$, $w \rightarrow 0$ or $u = 1 - v - w \rightarrow 0$, so no subtraction is needed for these two integrals. For the Fourier integral b_y , although we resolve the Landau pole, the direct integration is still unstable. There are two approaches to improve it. The first one (approximate method) is to dress the integration with a suppression factor:

$$\Theta_{\text{cut}} = \theta(b_{\text{cut}} - b_y) + \theta(b_y - b_{\text{cut}})e^{-\eta b_y}, \quad \text{with } b_{\text{cut}} = 2 \text{ GeV}^{-1}, \eta = 1 \text{ GeV}, \quad (3.4)$$

such that the integration can be performed using Monte Carlo methods which exhibit rapid convergence. There is no canonical choice for the values of b_{cut} and η . As we will show below, however, the difference is tiny. The second approach (exact method), which is more rigorous, is to use Fourier integrators, e.g. `QAWF` method [96] or `DoubleExponential` method [97]. In this calculation, we adopt the `QAWF` implemented in `GSL` [98] library for convenience. At N³LL, since the two-loop hard function contains generalized polylogarithms, we use `FastGPL` [99] for their numerical evaluations.

resummation order	Γ_{cusp}	$\gamma_{j,s,r}$	boundary	$\beta[\alpha_s]$	accuracy	non-singular
LL	1-loop	–	tree	1-loop	$\alpha_s^n L^{2n}$	–
NLL	2-loop	1-loop	tree	2-loop	$\alpha_s^n L^{2n-1}$	–
NNLL	3-loop	2-loop	1-loop	3-loop	$\alpha_s^n L^{2n-3}$	LO _{EEEC}
N ³ LL	4-loop	3-loop	2-loop	4-loop	$\alpha_s^n L^{2n-5}$	NLO _{EEEC}

Table 1: Definition of the resummation order and their corresponding ingredients [100].

Lastly, we need to specify the order counting. As summarized in Tab. 1, our logarithmic counting follows from the standard counting in SCET since we have normalized the distribution by dividing σ_{LO} . Again, we emphasize that the LO EEEC distribution starts at $\mathcal{O}(\alpha_s^2)$ excluding the boundary term, and its singular expansion is already at NNLL level. Similarly, NLO logarithms are fully predicted only in the N³LL resummed result. In contrast, for dijet event shapes (e.g. thrust and C -parameter), the first matching order is LL/NLL+LO. After resummation, we will switch the normalization from σ_{LO} to the born cross-section with y_3 resolution cut for the final result, i.e.

$$\sigma_1 = \int dPS_3 |\mathcal{M}_{\gamma^* \rightarrow q\bar{q}g}|^2 \theta(y_3 > y_{\text{cut}}). \quad (3.5)$$

While this order counting convention has been used in many event shape calculations from SCET, we modify the jet function boundaries to improve the perturbative convergence. In the upper panel of Fig. 7, we use the standard fixed-order expansion of the jet function from Eq. (2.36) and evolve the resummed jet function in Eq. (2.41) from its canonical scale to some randomly chosen scale, e.g., $\mu = 2b_0/b_y$, $\nu = b_0/b_y$. The uncertainty bands are obtained by varying the jet scale μ_j^{can} by a factor of 2. We see that the gluon jet function exhibits poor perturbative convergence, as increasing the logarithmic order does not result in a decrease in the uncertainty bands, especially in the relatively large b_y (but still perturbative) regime. Our investigation shows that the one-loop gluon jet constant c_g^1 being numerically too large is responsible for this

problem. To resolve this issue, we prompt $(\frac{\alpha_s}{4\pi}) c_g^1$ to be an order $\mathcal{O}(\alpha_s^0)$ number and define $e_i^1 = 1 + \left(\frac{\alpha_s(\mu_j)}{4\pi}\right) c_i^1$. Replacing all c_i^1 with $\frac{e_i^1 - 1}{\alpha_s(\mu_j)/(4\pi)}$, we write the improved jet functions to be

$$\begin{aligned} J_q^{\text{imp.}} &= e_q^1 + \left(\frac{\alpha_s}{4\pi}\right) \left[-2C_F e_q^1 L_b L_\omega + L_b \left(3C_F e_q^1 + \left(\frac{11}{3} C_A - \frac{4}{3} T_f n_f \right) (e_q^1 - 1) \right) \right] + \mathcal{O}(\alpha_s^2), \\ J_g^{\text{imp.}} &= e_g^1 + \left(\frac{\alpha_s}{4\pi}\right) \left[-2C_A e_g^1 L_b L_\omega + L_b \left(\left(\frac{11}{3} C_A - \frac{4}{3} T_f n_f \right) (2e_g^1 - 1) \right) \right] + \mathcal{O}(\alpha_s^2). \end{aligned} \quad (3.6)$$

We then replace the standard jet function $J_i(\mu_j, \nu_j)$ in Eq. (2.41) by the improved ones $J_i^{\text{imp.}}(\mu_j, \nu_j)$, and again vary μ_j^{can} by a factor of 2. We see a much better perturbative convergence as shown in the lower panel of Fig. 7. Therefore, we will use the improved jet functions instead of the standard ones for the final resummation.

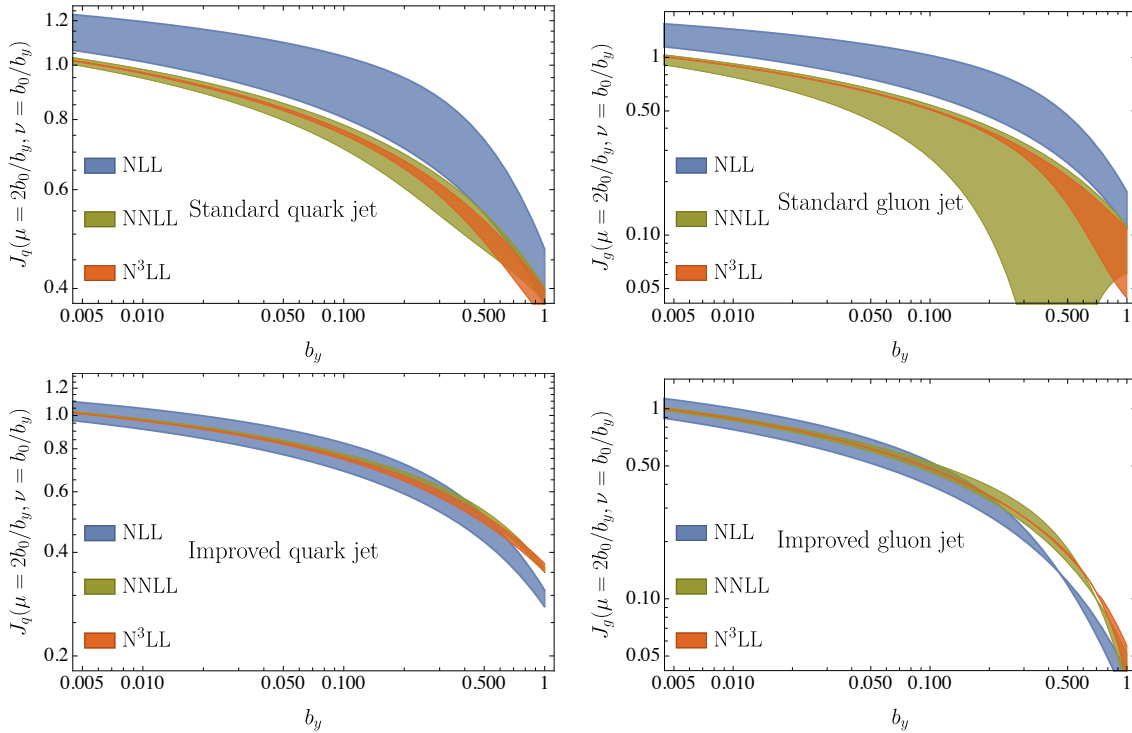


Figure 7: The perturbative convergence of resummed jet function. The upper panel shows the standard jet functions and the lower panel represents our improved jet functions. The uncertainty band is estimated by varying the canonical jet scale μ_j^{can} by a factor of 2. Note that $(\mu, \nu) = (2b_0/b_y, b_0/b_y)$ is randomly chosen for illustration; other choices would not change the behavior of bad/good convergence when varying μ_j^{can} .

With the above numerical setup, we calculate the central value of the resummation to N^3LL using both approximate and exact methods. Specifically, we set the relative error in QAWF to be 5×10^{-2} to reduce computational resource requirements. We show these two results in Fig. 8, where the solid lines represent the result with the exact method and the dashed lines are the predictions from the approximate method. Both approaches give consistent distributions for all

resummation orders. Moreover, we also calculate the relative difference, i.e. approximate/exact – 1, and show that it is within the error setting.

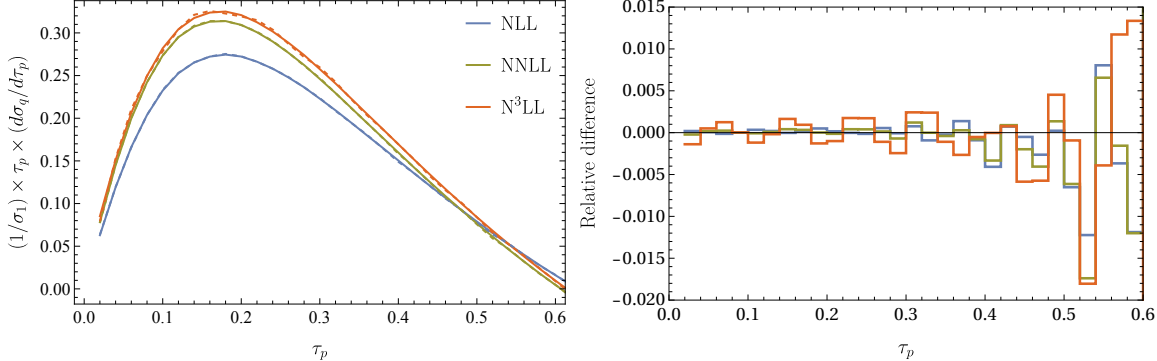


Figure 8: Left: Pure resummation to N^3LL . The solid lines use the exact method and the dashed lines use the approximate method. Both methods give consistent results. Right: the relative difference between the solid and dashed lines on the left. The errors are within 2% as expected.

Evaluating the Fourier integral b_y with QAWF requires a large amount of resources since we also have a two-dimensional Monte Carlo sampling for u and v . According to the aforementioned comparison, we can safely use the approximate method for the resummations.

3.3 Scale uncertainties

In this subsection, we study the scale uncertainties in order to check perturbative convergence and to estimate the higher-order effects. In practice, we introduce five parameters e_h , e_j , e_s , e_{rj} and e_{rs} to vary the hard, jet, soft, rapidity jet and rapidity soft scales, and they all range from 0.5 to 2. This amounts to modifying the canonical scales as follows:

$$\begin{aligned} \mu_h^{\text{can}} &= e_h Q, & \mu_j^{\text{can}} &= e_h e_j \frac{b_0}{b_y} \sqrt{1 + \frac{b_y^2}{b_{\max}^2} \frac{1}{e_h^2 e_j^2}}, & \mu_s^{\text{can}} &= e_h e_s \frac{b_0}{b_y} \sqrt{1 + \frac{b_y^2}{b_{\max}^2} \frac{1}{e_h^2 e_s^2}}, \\ \nu_j^{\text{can}} &= \mu_h^{\text{can}} e_{rj}, & \nu_s^{\text{can}} &= e_h e_{rs} \frac{b_0}{b_y} \sqrt{1 + \frac{b_y^2}{b_{\max}^2} \frac{1}{e_h^2 e_{rs}^2}} \end{aligned} \quad (3.7)$$

Note that the variation parameters inside the square root are to make sure $\mu_j, \mu_s, \nu_s \rightarrow \frac{b_0}{b_{\max}}$ when $b_y \rightarrow \infty$ no matter what the variation is. In other words, since b_{\max} is introduced to avoid the Landau pole and to control the non-perturbative corrections, it should not be affected by the perturbative uncertainty estimation. We also emphasize that the hard variation e_h is correlated among all the scales.

The scale variations follow the Higgs production calculation in Ref. [101]. The first type of variation is the hard scale e_h , where we vary all the scales by a factor of 2. The second type of variation is the resummation uncertainty. We choose all combinations of e_j , e_s , e_{rj} and e_{rs} while keeping $e_h = 1$. This generates $3^4 - 1 = 80$ possible variations. However, there are certain

combinations that double count the logarithm variations. For example, for $\ln \frac{\mu_s}{\nu_j}$ in Eq. (2.53), $e_s = 2$, $e_{rj} = 0.5$ gives a factor of 4. To avoid double counting, we require the variations to have

$$\left| \log_2 \frac{e_s}{e_j} \right|, \left| \log_2 \frac{e_s}{e_{rs}} \right|, \left| \log_2 \frac{e_{rj}}{e_{rs}} \right| \leq 1. \quad (3.8)$$

In addition, as pointed out in Ref. [101], the rapidity logarithms in Eq. (2.53) always show up in the combination of

$$\exp \left[(2C_F + C_A) \ln \frac{\nu_j^2}{\nu_s^2} \left(\frac{1}{2} \gamma_r [\alpha_s(b_0/b_y)] - A_\Gamma(\mu_j, b_0/b_y) \right) \right]. \quad (3.9)$$

Then a simultaneous variation of $e_j = 0.5$ with either $e_{rj} = 2$ or $e_{rs} = 0.5$ has already been accounted by the $\ln \frac{\nu_j}{\nu_s}$ variation. So we exclude these two combinations. Putting together, we get 35 scale variations and the final resummation uncertainty is the envelope of them.

In the left panel of Fig. 9, we show the pure resummation result from NLL to N^3LL for the coplanar EEEC. Increasing the resummation order reduces the uncertainty band as expected and the larger uncertainty from the lower-order resummation covers the higher-order band, indicating good perturbative convergence. In the right panel, we also show their relative difference to the best central curve, i.e. N^3LL prediction to illustrate the convergence.

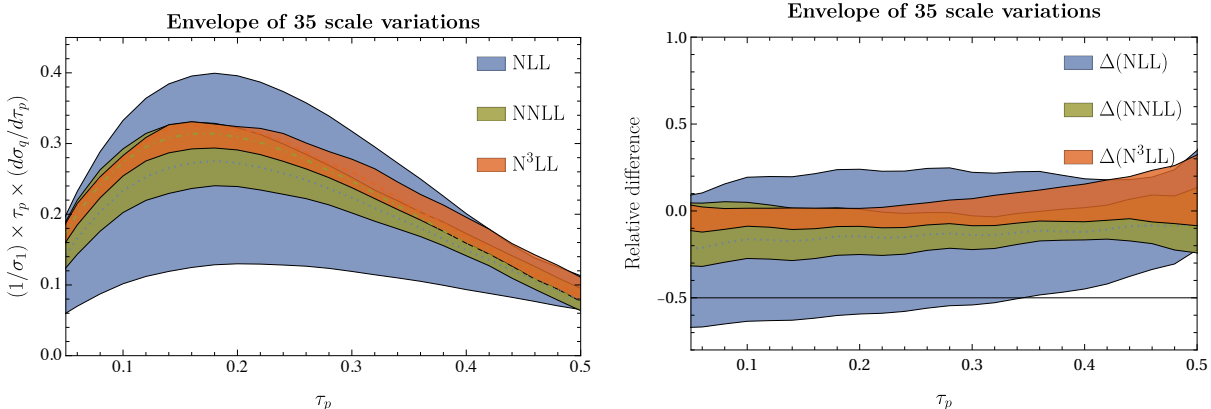


Figure 9: Left panel: final resummation result up to N^3LL accuracy with good perturbative convergence. Right panel: relative difference $\Delta(N^kLL) \equiv N^kLL/N^3LL - 1$.

In principle, we also need to match the perturbative resummation to the fixed-order predictions, i.e. add the non-singular contribution, and perform the renormalon subtraction. Particularly, to avoid double counting, a profile scale [48] is required to smoothly transform the resummation region into the fixed-order region. We will leave these for future work.

4 Resummation for three gluon jets

In this section, we study the resummation effects for the three gluon jets case, namely contributions initiated from the partonic process $e^+ e^- \rightarrow \gamma^* \rightarrow ggg$. Unlike the $q\bar{q}g$ case, the three-gluon

case is a loop-induced process and starts at two orders higher, i.e., $\mathcal{O}(\alpha_s^2)$ suppressed compared to the quark channel.

The factorization theorem is similar to Eq. (2.4), with the hard, fragmentation and soft functions replaced with those for the ggg case. The resummed formula then follows Eq. (2.52):

$$\frac{1}{\sigma_{\text{LO}}} \frac{d\sigma_g}{d\tau_p} = \int_T dv dw H_g(v, w, \mu_h) \int_{-\infty}^{\infty} \frac{db_y}{2\pi\xi} 2 \cos\left(\frac{b_y \tau_p}{\xi}\right) \times S_g(\mu_s, \nu_s) J_g(\mu_j, \nu_j) J_g(\mu_j, \nu_j) J_g(\mu_j, \nu_j) \times W_g(\mu_h, \mu_s, \nu_s, \mu_j, \nu_j), \quad (4.1)$$

and the RG kernel

$$\begin{aligned} W_g(\mu_h, \mu_s, \nu_s, \mu_j, \nu_j) &= \exp[6C_A(S_\Gamma(\mu_h, \mu_j) - S_\Gamma(\mu_s, \mu_j))] \\ &\times \exp[-2A_{\gamma_{h,g}}(\mu_h, \mu_s) + 2A_{\gamma_{J,g}}(\mu_s, \mu_j) + 2A_{\gamma_{J,g}}(\mu_s, \mu_j) + 2A_{\gamma_{J,g}}(\mu_s, \mu_j)] \\ &\times \left(\frac{Q^2}{\mu_h^2}\right)^{3C_A A_\Gamma(\mu_j, \mu_h)} \times \left(\frac{\nu_j^2}{\nu_s^2}\right)^{\frac{3C_A}{2}\gamma_r[\alpha_s(b_0/b_y)] - 3C_A A_\Gamma(\mu_j, b_0/b_y)} \\ &\times \left(\frac{\mu_s^2}{\nu_s^2}\right)^{3C_A A_\Gamma(\mu_j, \mu_s)} \times [(1-w)(1-v)]^{2C_A A_\Gamma(\mu_j, \mu_s)} (v+w)^{2C_A A_\Gamma(\mu_j, \mu_s)}. \end{aligned} \quad (4.2)$$

To have a consistent logarithmic counting in both channels, we start by building up some conventions below. First of all, if we define

$$r_q(\tau_p) \equiv \frac{1}{\sigma_{\text{LO}}} \frac{d\sigma_q}{d\tau_p}, \quad r_g(\tau_p) \equiv \frac{1}{\sigma_{\text{LO}}} \frac{1}{\alpha_s^2} \frac{d\sigma_g}{d\tau_p} \quad (4.3)$$

then the distribution strictly follows the counting in Tab. 1, where the $N^k\text{LL}$ accuracy in $r_i(\tau_p)$ corresponds to $\alpha^n L^{2n} \sim \alpha_s^n L^{2n-(2k-1)}$. More importantly, we can use the same convention for all ingredients in the ggg channel resummation. Then to obtain the sum of the distribution, $\frac{1}{\sigma_{\text{LO}}} \frac{d\sigma}{d\tau_p} = r_q(\tau_p) + \alpha_s^2 r_g(\tau_p)$, we need to determine what logarithmic order in $r_g(\tau_p)$ is as important as the $N^k\text{LL}$ order of $r_q(\tau_p)$. It turns out that up to NNLL accuracy, there is no ggg channel required, and for $N^k\text{LL}$ accuracy with $k \geq 3$, we need to add $N^{k-2}\text{LL}$ resummation from ggg channel. That is to say, our $N^3\text{LL}$ resummation in the $q\bar{q}g$ case requires corrections from NLL in ggg channel.

At NLL, we need the two-loop cusp anomalous dimension, one-loop regular hard, jet, and soft anomalous dimensions, and the LO three-gluon hard function. First of all, the LO hard function is simply the first order differential cross section for $e^+e^- \rightarrow ggg$ [102, 103]. An example Feynman diagram can be found in Fig. 10. The hard function for $e^+e^- \rightarrow ggg$ satisfies the same RG equation as shown in Eq. (2.27). By evaluating the right-hand side of Eq. (2.27) for three gluon final states, i.e.,

$$\begin{aligned} \mathbf{T}_1 \cdot \mathbf{T}_2 = \mathbf{T}_1 \cdot \mathbf{T}_3 = \mathbf{T}_2 \cdot \mathbf{T}_3 = -\frac{1}{2}\mathbf{T}_1^2 = -\frac{1}{2}\mathbf{T}_2^2 = -\frac{1}{2}\mathbf{T}_3^2 = -\frac{1}{2}C_A, \\ f_{abe} f_{cde} \sum_{i=1}^3 \sum_{\substack{1 \leq j < k \leq 3 \\ j, k \neq i}} \{\mathbf{T}_i^a, \mathbf{T}_i^d\} \mathbf{T}_j^b \mathbf{T}_k^c |ggg\rangle = 9C_A |ggg\rangle, \end{aligned} \quad (4.4)$$

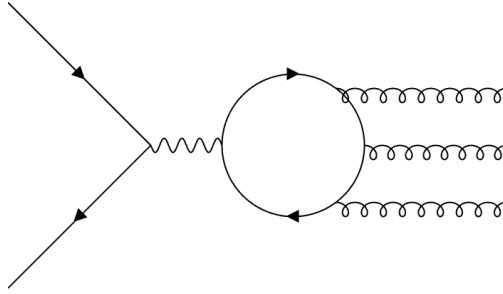


Figure 10: An example diagram of the $e^+e^- \rightarrow \gamma^* \rightarrow ggg$ process. Squaring this amplitude results in an $\mathcal{O}(\alpha_s^2)$ suppression.

the Eq. (2.31) becomes

$$\frac{d \ln H_g(v, w, \mu)}{d \ln \mu^2} = \frac{3C_A}{2} \gamma_{\text{cusp}}(\alpha_s) \ln \frac{Q^2}{\mu^2} + \gamma_{h,g}(v, w, \alpha_s), \quad (4.5)$$

where the non-cusp piece for three gluons is

$$\begin{aligned} \gamma_{h,g}(v, w, \alpha_s) = & \gamma_{\text{cusp}}(\alpha_s) \frac{C_A}{2} (\ln v + \ln w + \ln(1 - v - w)) \\ & + 3\gamma_g(\alpha_s) + 9C_A\gamma_{\text{quad}}[\alpha_s]. \end{aligned} \quad (4.6)$$

We emphasize that the $\gamma_{\text{quad}}(\alpha_s)$ starts at $\mathcal{O}(\alpha_s^3)$ and will not contribute until N³LL.

The soft function for the three gluons process has the same form as in Eq. (2.42), and satisfies the same RG equation in Eq. (2.44)-(2.45). Using Eq. (4.4) and Eq. (2.46), the soft RG in Eq. (2.47)-(2.48) become

$$\frac{d \ln S_g}{d \ln \mu^2} = \frac{3C_A}{2} \left(\gamma_{\text{cusp}}[\alpha_s] \ln \frac{\mu^2}{\nu^2} - \gamma_s[\alpha_s] \right) + \frac{C_A}{2} \gamma_{\text{cusp}}[\alpha_s] \ln \frac{(v+w)^2(1-v)^2(1-w)^2}{vw(1-v-w)} - 9C_A\gamma_{\text{quad}}[\alpha_s], \quad (4.7)$$

$$\frac{d \ln S_g}{d \ln \nu^2} = \frac{3C_A}{2} \left(\int_{\mu^2}^{b_0^2/b_y^2} \frac{d\bar{\mu}^2}{\bar{\mu}^2} \gamma_{\text{cusp}}(\alpha_s[\bar{\mu}]) + \gamma_r(\alpha_s[b_0/b_y]) \right). \quad (4.8)$$

With all the ingredients at hand, we now perform the Fourier integral in Eq. (4.1) with the same setup in the $q\bar{q}g$ channel, namely the approximate method in Eq. (3.4). We also use the envelope of 35 variations to estimate the uncertainty band. The distribution is normalized to σ_1 for consistency as in the $q\bar{q}g$ channel. In Fig. 11, we show both the NLL resummation including the perturbative uncertainty band and its ratio to the N³LL resummation in the $q\bar{q}g$ channel. The contribution from the ggg channel is relatively small: only 0.02% correction to our highest-order resummation in the range $0 < \tau_p \leq 0.5$. This is expected because the hard function is already suppressed by α_s^2 . While the comparison suggests we can ignore the ggg channel in the current study, we want to emphasize the existence of this additional channel in N³LL and beyond, which could become phenomenologically relevant in future scenarios, e.g. when looking at the next-to-leading power corrections. To our knowledge, our result is the first resummation for three gluon jets at e^+e^- .

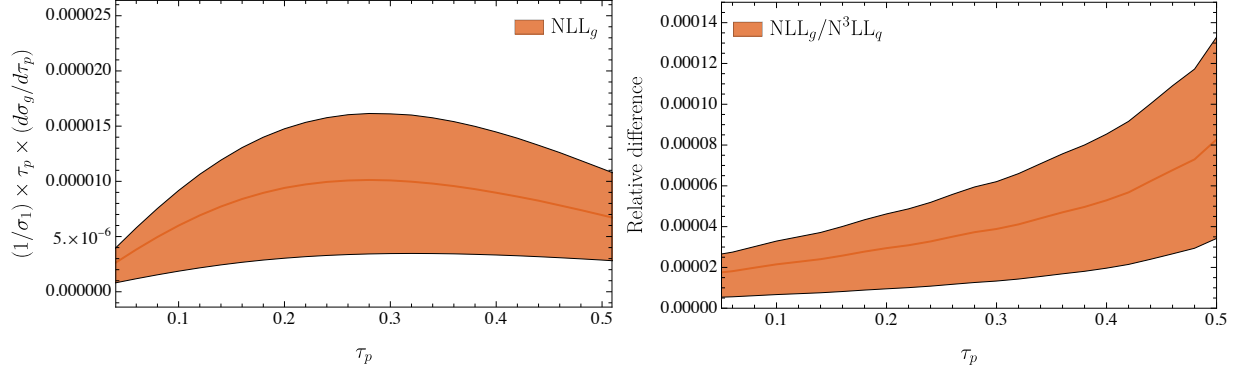


Figure 11: Left: NLL resummation for $e^+e^- \rightarrow \gamma^* \rightarrow ggg$ process. Right: the relative difference between this NLL resummation and the N^3LL resummation of the $q\bar{q}g$ channel. Note that because the $q\bar{q}g$ cross-section is close to zero near $\tau_p = 0.5$, the relative difference starts to increase.

5 Fully differential EEEC in the coplanar limit

In this section, we study the three-particle coplanar limit in the fully differential EEEC as defined in Eq. (1.1) with $n = 3$. Below we will briefly review the variables $\{s, \phi_1, \phi_2\}$ and consider the $s \rightarrow 1$ limit. Then we will explore the resummation effects of different coplanar configurations, which are characterized by the angles $\{\phi_1, \phi_2\}$.

To begin with, we review the celestial coordinate introduced in Ref. [15]. For any three final-state particles, if we label the angles between any pair of them to be θ_{ij} , then we can map them to three points on the celestial sphere:

$$\frac{1 - \cos \theta_{ij}}{2} = \frac{|y_i - y_j|^2}{(1 + |y_i|^2)(1 + |y_j|^2)}, \quad i \neq j \in \{1, 2, 3\}. \quad (5.1)$$

Using these three points $y_{1,2,3}$, we can construct a circle and define the radius \sqrt{s} as well as two angles $\phi_{1,2}$ for y_1 and y_2 , as shown in Fig. 12. This amounts to the following formulae

$$y_1 = \sqrt{s}e^{i\phi_1}, \quad y_2 = \sqrt{s}e^{i(\phi_1+\phi_2)}, \quad y_3 = \sqrt{s}. \quad (5.2)$$

On the one hand, $s \rightarrow 0$ will force θ_{ij} goes to zero homogeneously and approaches the collinear limit. On the other hand, in the $s \rightarrow 1$ limit, the three particles fall onto the same plane, with $\theta_{13} = \phi_1$, $\theta_{21} = \phi_2$, $\theta_{32} = 2\pi - \phi_1 - \phi_2$. Large logarithms of $\ln(1 - s)$ in the EEEC were noticed through fixed-order calculations [13–15]. In particular, the leading-power contribution in the three-particle coplanar limit ($s \rightarrow 1$) with fixed ϕ_1, ϕ_2 is governed by the trijet coplanar configuration where ϕ_1, ϕ_2 characterize the relative angles between pairs of the three jets⁵. Therefore, in this limit, $\{\tau, u, v\}$ and $\{s, \phi_1, \phi_2\}$ are interchangeable, and we can convert the factorization theorem in the $\tau_p \rightarrow 0$ limit to the one for $s \rightarrow 1$ limit. We find

$$\tau_p = 2(1 - s) \sin \frac{\phi_1}{2} \sin \frac{\phi_2}{2} \sin \frac{(\phi_1 + \phi_2)}{2},$$

⁵Notice that the trijet configuration requires ϕ_1, ϕ_2 satisfy $\phi_1 < \pi, \phi_2 < \pi, \phi_1 + \phi_2 > \pi$. Therefore, there is no large $\ln(1 - s)$ in regions outside $\phi_1 < \pi, \phi_2 < \pi, \phi_1 + \phi_2 > \pi$, as noticed in Ref. [14].

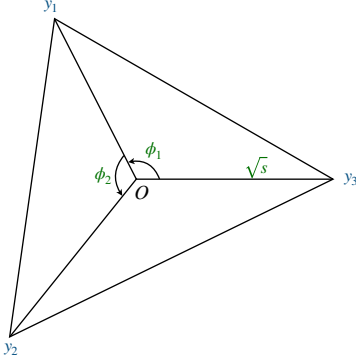


Figure 12: Demonstration of celestial coordinate. By mapping the angular distances to three points $y_{1,2,3}$ on the celestial sphere, we introduce the radius s and two angle variables $\phi_{1,2}$.

$$\{u, v, w\} \in \{z_i\} = \left\{ \cot \frac{\phi_1}{2} \cot \frac{\phi_2}{2}, -\cot \frac{\phi_1}{2} \cot \frac{(\phi_1 + \phi_2)}{2}, -\cot \frac{\phi_2}{2} \cot \frac{(\phi_1 + \phi_2)}{2} \right\}, \quad (5.3)$$

where u, v, w can take any order of the three terms $\{z_i\}$ from the right-hand side, corresponding to the S_3 symmetry of EEEC. From Eq. (5.3), we can write ξ in Eq. (2.2) as

$$\xi = \frac{4}{Q} \sin \frac{\phi_1}{2} \sin \frac{\phi_2}{2} \sin \frac{(\phi_1 + \phi_2)}{2} = \frac{2\tau_p}{Q(1-s)}. \quad (5.4)$$

Therefore, in order to derive the factorization theorem for the fully differential EEEC in the $s \rightarrow 1$ limit, we can convert from the factorization formula for τ_p in Eq. (2.21) rather than starting from scratch. First, we account for the Jacobian factor

$$\left| \frac{\partial(\tau_p, u, v)}{\partial(s, \phi_1, \phi_2)} \right| = -\cot \frac{\phi_1}{2} \cot \frac{\phi_2}{2} \cot \frac{(\phi_1 + \phi_2)}{2}. \quad (5.5)$$

In addition, instead of normalizing by the jet energies $E_{J_1}E_{J_2}E_{J_3}$ as in Eq. (1.4), here the normalization factor is Q^3 , which results in an extra factor

$$\begin{aligned} \frac{E_{J_1}E_{J_2}E_{J_3}}{Q^3} &= -\frac{\sin \phi_1 \sin \phi_2 \sin(\phi_1 + \phi_2)}{(\sin \phi_1 + \sin \phi_2 - \sin(\phi_1 + \phi_2))^3} \\ &= -\frac{1}{8} \cot \frac{\phi_1}{2} \cot \frac{\phi_2}{2} \cot \frac{(\phi_1 + \phi_2)}{2} \csc \frac{\phi_1}{2} \csc \frac{\phi_2}{2} \csc \frac{(\phi_1 + \phi_2)}{2}. \end{aligned} \quad (5.6)$$

Accounting for all these factors and the S_3 symmetry, we obtain the factorization formula for the $q\bar{q}g$ channel in the $s \rightarrow 1$ limit for the fully differential spectrum,

$$\begin{aligned} \frac{1}{\sigma_{\text{LO}}} \frac{d^3\sigma_q}{ds d\phi_1 d\phi_2} &= \frac{Q}{8} \left[\cot \frac{\phi_1}{2} \cot \frac{\phi_2}{2} \cot \frac{(\phi_1 + \phi_2)}{2} \csc \frac{\phi_1}{2} \csc \frac{\phi_2}{2} \csc \frac{(\phi_1 + \phi_2)}{2} \right]^2 \times \sum_{i,j,k} H_q(z_i, z_j, z_k, \mu) \\ &\times \int_0^\infty \frac{db_y}{2\pi} \cos \left(\frac{b_y Q(1-s)}{2} \right) \times S_q(b_y, \mu, \nu) J_q(b_y, \mu, \nu) J_{\bar{q}}(b_y, \mu, \nu) J_g(b_y, \mu, \nu), \end{aligned} \quad (5.7)$$

where i, j, k run over all six permutations and we emphasize that there is z_i dependence in the hard anomalous dimensions. The ggg channel again takes a similar factorized form with associated ingredients. Solving RGEs for hard, jet, and soft functions are identical to the τ_p case and so is the final resummed form, therefore we don't write them down here.

The advantage of studying a fully differential spectrum is that setting different values of $\phi_{1,2}$ allows us to study different coplanar configurations (or trijet shapes). For example, $\phi_1 = \phi_2 = 2\pi/3$ represents the symmetric trijet configuration and $\phi_1 \rightarrow 0$ or $\phi_2 \rightarrow 0$ or $\phi_1 + \phi_2 \rightarrow \pi$ corresponds to the squeezed limit, where there are two jets collinear with each other and the third jet being backward.

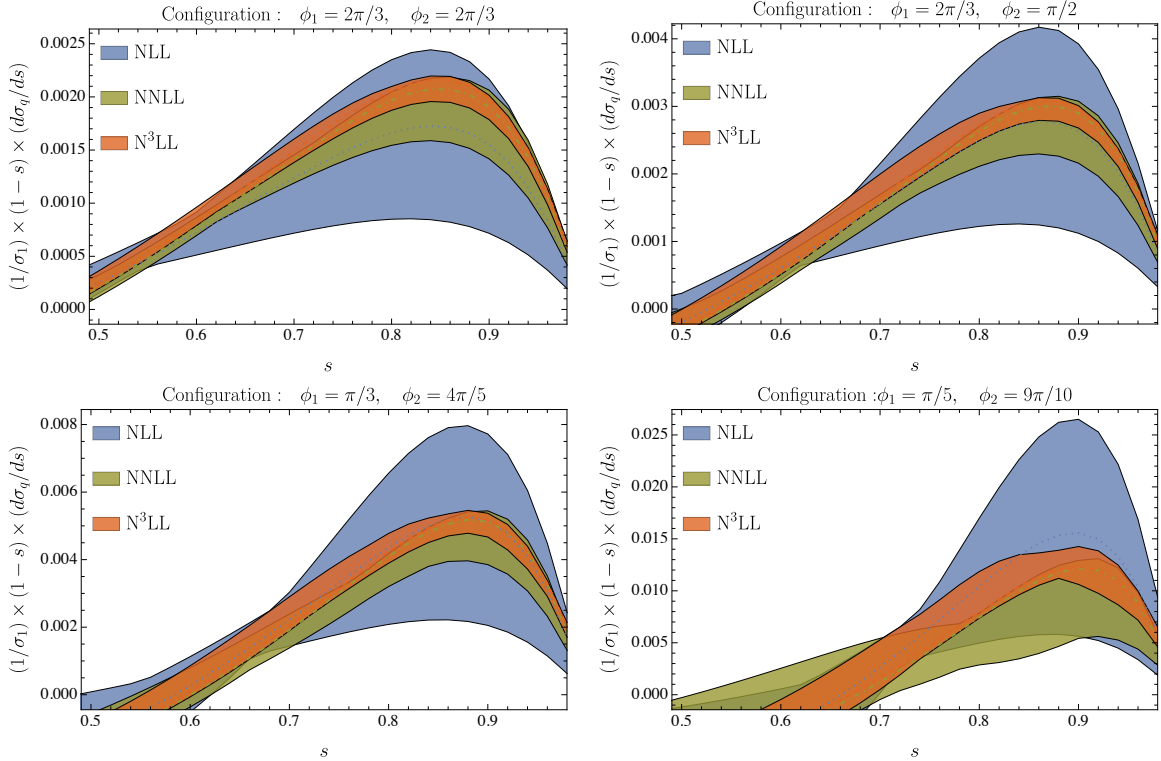


Figure 13: Resummation of fully differential spectrum with four configurations. For each configuration, we find good convergence in the resummation orders.

In Fig. 13, we show the resummation results for four choices of $\{\phi_1, \phi_2\}$: $\{2\pi/3, 2\pi/3\}$, $\{2\pi/3, \pi/2\}$, $\{\pi/3, 4\pi/5\}$ and $\{\pi/5, 9\pi/10\}$. The first one corresponds to the exact symmetric configuration, the second and the third are regular configurations, and the last one approaches the squeezed limit. While the higher-order band mostly falls into the lower-order one in the first three cases, we observed slightly poor convergence in the last configuration. In particular, the distribution goes to negative faster than others, indicating that we should turn off the resummation below $s \sim 0.7$. This is reasonable because the cross-section also receives additional logarithms in the squeezed limits, e.g. $\ln(\tan^2 \frac{\phi_1}{2} \tan^2 \frac{\phi_2}{2} \tan^2 \frac{\phi_1+\phi_2}{2})$. In principle, these logarithms need to be resummed in the fully differential spectrum but we leave it for future work. On the contrary,

in the τ_p spectrum, the jet algorithm protects us from the squeezed singularities and thus we do not observe these effects.

6 Analysis

In this section, we perform some further studies. In Sec. 6.1, we explore the non-perturbative power corrections using the Monte Carlo program **Pythia8** [104]. In Sec. 6.2, we show a simple relation between the τ_p -projected EEEC with the D -parameter.

6.1 Non-perturbative corrections

So far we are only studying the perturbative predictions for coplanar EEEC, while experiments will measure the observable on hadrons. There are different ways to turn the partonic predictions into hadronic results that can be compared with the experimental data. In general, the non-perturbative power corrections to the event shape observables are suppressed by Λ_{QCD}/Q , where Q is the center-of-mass energy. In the current collider programs, many analyses use the Monte Carlo generators to estimate the non-perturbative effects from the hadronization process. On the other hand, there are also analytic approaches, such as renormalon-based calculation [105] and SCET-based OPE analysis [106, 107], to extract the leading power corrections to a specific QCD observable.

It will be interesting to rigorously study these effects for coplanar EEEC using the operator language in SCET, but in this paper, we first present a qualitative analysis of the hadronization effect using **Pythia8** [104] with **FastJet** interface [108]. In the numerical setup, we sample 10 million events in **Pythia8**, select the three-jet events with k_T algorithm implemented in **FastJet**, and calculate coplanar EEEC τ_p before and after the hadronization. To be consistent, we also set $\alpha_s = 0.118$ and the y_3 cutoff to be $y_{\text{cut}} = 0.1$. To illustrate the size of hadronization correction, we then calculate the ratio difference of the spectrum, i.e. $\Delta(d\sigma/d\tau_p) = (d\sigma^{\text{hadron}}/d\tau_p)/(d\sigma^{\text{parton}}/d\tau_p) - 1$ bin by bin.

In Fig. 14, we show the distribution from **Pythia8** at $Q = 91.2\text{GeV}$ and $Q = 250\text{GeV}$, where the latter corresponds to the energy for CEPC. Because the parton shower and hadronization model include more things than our fixed-order calculation or the analytic resummation, we normalize the **Pythia8** spectrum by integration of the distribution itself, i.e. instead of σ_1 , we use $\sigma = \int_0^1 d\tau_p (d\sigma^{\text{parton/hadron}}/d\tau_p)$. We find that the hadronization correction $\Delta(d\sigma/d\tau_p)$ is less than 15% for $Q = 91.2$ GeV and less than 8% for $Q = 250$ GeV. In the small τ_p region, we learn from the coplanar resummation that the smallest scale is $\mu_j = \mu_s = b_0/b_y \sim \tau_p Q$. Then we would qualitatively expect the non-perturbative correction in powers of $\Lambda_{\text{QCD}}/(\tau_p Q)$, which is consistent with the $\tau_p < 0.2$ region in the lower panels of Fig. 14.

To study the Q dependence of the hadronization effects, we also choose a few τ_p values and calculate the hadronization correction $\Delta(d\sigma/d\tau_p)$ with different energies Q , ranging from 20 GeV to 1 TeV. As shown in Fig. 15, when τ_p is small ($\tau_p = 0.015, 0.035, 0.055, 0.075$) or large ($\tau_p = 0.495, 0.595, 0.795, 0.895$), the size of hadronization correction decreases as the energy Q increases, though they have opposite signs. This is also consistent with the argument that non-perturbative correction is suppressed by powers of Λ_{QCD}/Q . However, there exists a transition

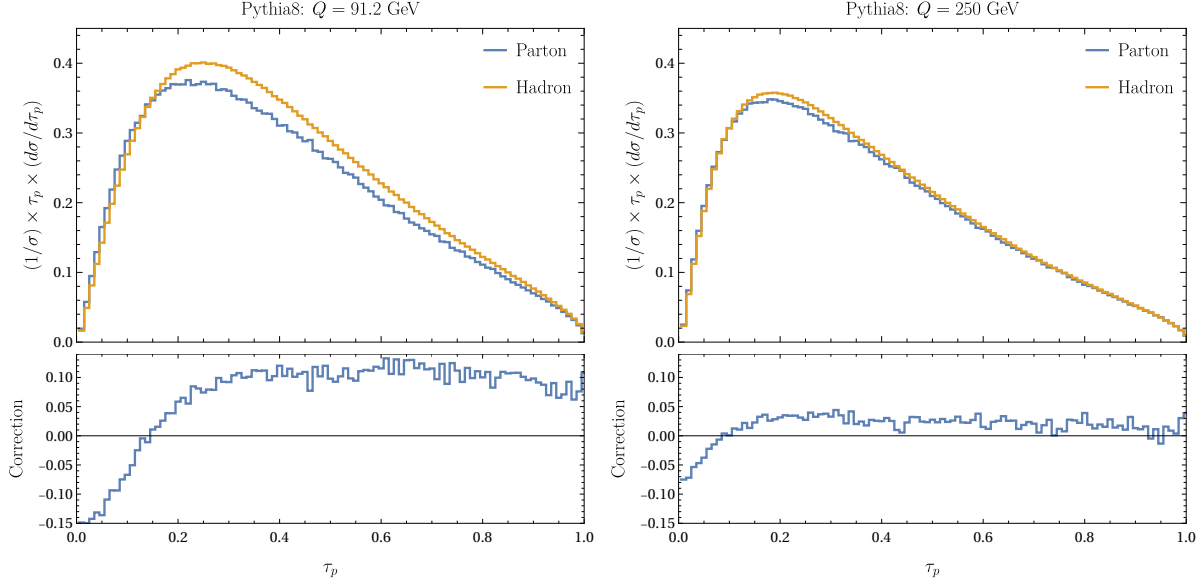


Figure 14: Partonic and hadronic distributions of the coplanar EEEC in Pythia8, with $Q = 91.2$ GeV and $Q = 250$ GeV.

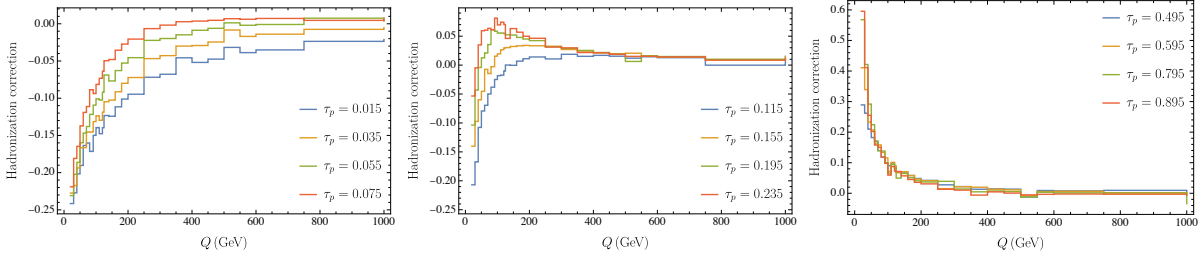


Figure 15: Q dependence of hadronization correction with τ_p fixed. In these three plots, we focus on the small, middle, and large τ_p regions of the distribution, and observe a transition of Q dependence in the middle region.

region around $\tau_p = 0.2$ that exhibits different Q dependence. It will be interesting to derive the trijet operator using SCET and study the hadronization effect quantitatively in the Fourier space. We leave them for future work.

6.2 Relation between D -Parameter and τ_p -projected EEEC

As mentioned in the introduction, the D -parameter is also a canonical event shape to study the coplanar trijet configuration. As an aside, in this subsection, we derive a simple relation between the third moment of the τ_p -projected EEEC defined in Eq. (1.3) and the D -parameter.

In massless QCD, the C -parameter and the D -parameter are defined as [109–111],

$$C = 3(\lambda_1\lambda_2 + \lambda_1\lambda_3 + \lambda_2\lambda_3), \quad D = 27\lambda_1\lambda_2\lambda_3, \quad (6.1)$$

where λ_i are the three eigenvalues of the spherocity tensor $\Theta_{\alpha\beta}$,

$$\Theta_{\alpha\beta} = \frac{1}{Q} \sum_i \frac{k_{i\alpha} k_{i\beta}}{E_i}, \quad (6.2)$$

Here i runs over all final-state particles. Q here is the center-of-mass energy, E_i is the energy of particle i , and $k_{i\alpha}$ is the α component of particle i 's three momentum ($\alpha, \beta = 1, 2, 3$).

Writing the D -parameter in terms of $\text{Tr } \Theta (= 1)$, $\text{Tr } \Theta^2$ and $\text{Tr } \Theta^3$, we find

$$\begin{aligned} D &= \frac{27}{6} \left\{ (\lambda_1 + \lambda_2 + \lambda_3) \left[(\lambda_1 + \lambda_2 + \lambda_3)^2 - 3(\lambda_1^2 + \lambda_2^2 + \lambda_3^2) \right] + 2(\lambda_1^3 + \lambda_2^3 + \lambda_3^3) \right\} \\ &= \frac{27}{6} \left\{ \text{Tr } \Theta \left[(\text{Tr } \Theta)^2 - 3 \text{Tr } \Theta^2 \right] + 2 \text{Tr } \Theta^3 \right\} \\ &= \frac{27}{6} \left(1 - 3 \sum_{i,j} \frac{E_i E_j \cos^2 \theta_{ij}}{Q^2} + 2 \sum_{i,j,k} \frac{E_i E_j E_k \cos \theta_{ij} \cos \theta_{jk} \cos \theta_{ki}}{Q^3} \right) \\ &= \frac{27}{Q^3} \sum_{i < j < k} E_i E_j E_k (1 + 2 \cos \theta_{ij} \cos \theta_{jk} \cos \theta_{ki} - \cos^2 \theta_{ij} - \cos^2 \theta_{jk} - \cos^2 \theta_{ki}) \\ &= \frac{27}{Q^3} \sum_{i < j < k} \frac{\left| (\vec{k}_i \times \vec{k}_j) \cdot \vec{k}_k \right|^2}{E_i E_j E_k} \\ &= \frac{27}{Q^3} \sum_{i < j < k} E_i E_j E_k \tau_{ijk}^2. \end{aligned} \quad (6.3)$$

Therefore, the average of the D -parameter is proportional to the second moment of our τ_p -projected EEEC,

$$\langle D \rangle = \frac{9}{2} \int_0^1 d\tau_p \tau_p^2 \frac{1}{\sigma_{\text{tot}}} \frac{d\sigma}{d\tau_p}, \quad (6.4)$$

where σ_{tot} is the total cross section.

A similar relation also exists between the C -parameter and the EEC (noticed in e.g. Ref. [112]). We also derive it here,

$$C = \frac{3}{2} \left[(\lambda_1 + \lambda_2 + \lambda_3)^2 - (\lambda_1^2 + \lambda_2^2 + \lambda_3^2) \right] \quad (6.5)$$

$$\begin{aligned} &= \frac{3}{2} [1 - \text{Tr}(\Theta^2)] \\ &= \frac{3}{2} \left(1 - \sum_{i,j} \frac{E_i E_j \cos^2 \theta_{ij}}{Q^2} \right), \end{aligned} \quad (6.6)$$

Therefore, we find that the average of the C -parameter is related to the moments of the EEEC by

$$\langle C \rangle = \frac{3}{2} \left(1 - \int_0^1 dx (1 - 2x)^2 \frac{1}{\sigma_{\text{tot}}} \frac{d\sigma}{dx} \right) = 6 \int_0^1 dx x(1-x) \frac{1}{\sigma_{\text{tot}}} \frac{d\sigma}{dx}, \quad (6.7)$$

where x is x_{12} in Eq. (1.1).

Inspired by these relations, it will be interesting to generalize the factorization theorem developed for the EEC and the coplanar EEEC to the trijet region of both C -parameter and D -parameter in the future.

7 Conclusion

Precise measurements for the Standard Model, in particular QCD and the Higgs sector, have been one of the primary tasks in collider physics, for both improving our understanding of quantum field theories and helping with new physics searches. In recent years, energy correlators have opened up a new precision era for both e^+e^- and proton-proton colliders. First of all, the energy correlator has a very simple definition compared to other jet observables and thus allows for accurate theoretical predictions from higher-order computations. Secondly, the energy correlator can be defined both perturbatively and non-perturbatively, which makes it an ideal observable to study non-perturbative power corrections. Particularly, it connects the QFT operators and CFT techniques to phenomenological studies and real-world experiments (see Refs. [113–118]). Lastly, there are various infrared limits in the multi-point energy correlators as discussed in Ref. [13], such as collinear, squeezed, and coplanar limits. It is a playground for developing EFT techniques and applying them to precision QCD measurements.

In this paper, we propose a new projection τ_p of the three-point energy correlator and study the coplanar limit from the $\tau_p \rightarrow 0$ region. In particular, we focus on the so-called trijet configuration where there are three well-separated jets falling on the same plane, and to guarantee infrared safety, we identify these three jets by the k_T algorithm. From trijet kinematics of $e^+e^- \rightarrow \gamma^* \rightarrow q\bar{q}g$, i.e. the effects of collinear splitting and soft recoil, we derive a TMD-based factorization in SCET to describe the large logarithms enhancement $\ln(\tau_p)$ in this region. It turns out to be a natural generalization of the back-to-back factorization for a two-point correlator, EEC, where the collinear dynamics are captured by the TMD fragmentation function, and the soft emissions are organized into the trijet TMD soft function.

The only missing ingredient to achieve N^3LL resummation is the two-loop $q\bar{q}g$ hard function, which we extract from the QCD form factors in the literature. Then we solve the RGEs for individual ingredients and perform the resummation for coplanar EEC in the $\gamma^* \rightarrow q\bar{q}g$ channel. To our best knowledge, this is the first trijet observable that reaches the N^3LL accuracy. We also estimate the perturbative uncertainties by varying all the renormalization scales systematically and find a good convergence from NLL to N^3LL . This is the main result of the paper. For completeness, we also look into the resummation for the $\gamma^* \rightarrow ggg$ channel. Since it is $\mathcal{O}(\alpha_s^2)$ suppressed relative to the $\gamma^* \rightarrow q\bar{q}g$ channel, one should add the $N^{k-2}LL$ resummation as correction to the $q\bar{q}g$ channel at N^kLL accuracy. We therefore compute it to NLL and compare it with N^3LL $q\bar{q}g$ channel. We also emphasize that this is the first resummation program for the “light-by-glue”, $\gamma^* \rightarrow ggg$ channel.

In Refs. [13–15], we proposed another way of probing the coplanar limit, i.e. $s \rightarrow 1$ limit under the celestial parameterization, which is referred to as fully differential spectrum in this paper. We generalize our τ_p factorization to the fully differential case and also perform the N^3LL resummation for $\ln(1-s)$ logarithms for fixed trijet shapes (i.e. fixed ϕ_1 and ϕ_2). For a generic value of $\phi_{1,2}$, we find similar distributions as the τ_p projection and good convergence. However, when approaching the squeezed limit, we receive additional enhancement from logarithms of $\phi_{1,2}$ and they also need to be resummed. It will be interesting to study the factorization for the squeezed limit and explore the joint resummation with the coplanar limit.

As mentioned in Sec. 2, the factorization theorem and resummation we derived can be applied

to other processes, such as Higgs decays and Z decays, and the only required change is the hard function. Although the data from the Large Electron-Position Collider might not have enough trijet events to perform these analyses, future colliders like CEPC, ILC and FCC-ee will allow the precise measurements of coplanar EEEC. On the one hand, the more inclusive spectrum, τ_p projection, can be applied to the extractions of Standard Model parameters, e.g. the strong coupling constant α_s , Higgs mass and Yukawa couplings. On the other hand, the fully differential spectrum provides access to different hard kinematics and can contribute to removing the QCD backgrounds in the data. Moreover, it will be interesting to apply our factorization to the boosted top decay, where the decay particles will be formed into three QCD jets on the same plane in the top rest frame. The coplanar resummation will then improve the theoretical prediction of the Jacobian peak of the top decay EEEC and help with the top quark mass extraction at the LHC.

Acknowledgments

We would like to thank Hua Xing Zhu for collaboration at the early stage of this project. We also thank Arindam Bhattacharya, Miguel Benitez, Kyle Lee, Johannes Michel, Ian Moult, Matthew Schwartz, Iain Stewart and Hua Xing Zhu for useful discussions. A.G. was supported by the U.S. Department of Energy, Office of Science, Office of Nuclear Physics, from DE-SC0011090. T.-Z.Y wants to acknowledge the European Research Council (ERC) for the funding under the European Union’s Horizon 2020 research and innovation programme grant agreement 101019620 (ERC Advanced Grant TOPUP). XY.Z. was supported in part by the U.S. Department of Energy under contract DE-SC0013607.

A Running coupling and RG kernels

In this section, we summarize the running coupling and the RG kernels in the resummation setup. The beta function is given as follows

$$\frac{d\alpha_s(\mu)}{d \ln \mu} = \beta(\alpha_s(\mu)), \quad \beta(\alpha) = -2\alpha \left[\left(\frac{\alpha}{4\pi} \right) \beta_0 + \left(\frac{\alpha}{4\pi} \right)^2 \beta_1 + \left(\frac{\alpha}{4\pi} \right)^3 \beta_2 + \dots \right], \quad (\text{A.1})$$

where the coefficient up to three loops are given by [119–122]

$$\begin{aligned} \beta_0 &= \frac{11}{3} C_A - \frac{4}{3} T_F n_f, \\ \beta_1 &= \frac{34}{3} C_A^2 - \frac{20}{3} C_A T_F n_f - 4 C_F T_F n_f, \\ \beta_2 &= n_f^2 T_F^2 \left(\frac{158}{27} C_A + \frac{44}{9} C_F \right) + n_f T_F \left(2C_F^2 - \frac{205}{9} C_F C_A - \frac{1415}{27} C_A^2 \right) + \frac{2857}{54} C_A^3, \\ \beta_3 &= \frac{1093}{729} n_f^3 + \left(\frac{50065}{162} + \frac{6472}{81} \zeta_3 \right) n_f^2 + \left(-\frac{1078361}{162} - \frac{6508}{27} \zeta_3 \right) n_f + 3564 \zeta_3 + \frac{149753}{6}. \end{aligned} \quad (\text{A.2})$$

At one-loop, Eq. (A.1) can be solved exactly. At two-loop and beyond, there are different solutions. In this paper, we use the so-called iterative solution, where the RGE is solved iteratively

order-by-order in the expansion of β_n/β_0 . Explicitly, the four-loop running coupling needed for the N³LL resummation is

$$\begin{aligned} \alpha_s(\mu) = \alpha_s(Q) & \left\{ X + \frac{\alpha_s(Q)}{4\pi} \frac{\beta_1}{\beta_0} \ln X + \frac{\alpha_s^2(Q)}{16\pi^2} \left[\frac{\beta_2}{\beta_0} \left(1 - \frac{1}{X} \right) + \frac{\beta_1^2}{\beta_0^2} \left(\frac{1}{X} - 1 + \frac{\ln X}{X} \right) \right] \right. \\ & \left. + \frac{\alpha_s^3(Q)}{64\pi^3} \left[\frac{\beta_3}{2\beta_0} \left(1 - \frac{1}{X^2} \right) + \frac{\beta_1\beta_2}{\beta_0^2} \left(\frac{1-X}{X} + \frac{\ln X}{X^2} \right) + \frac{\beta_1^3}{2\beta_0^3} \left(1 + \frac{1}{X^2} - \frac{2}{X} - \frac{\ln^2 X}{X^2} \right) \right] \right\}^{-1} \end{aligned} \quad (\text{A.3})$$

where

$$X \equiv 1 + \frac{\alpha_s(Q)}{2\pi} \beta_0 \ln \frac{\mu}{Q} \quad (\text{A.4})$$

Note that the two-loop and three-loop running needed for lower-order resummation can be obtained by only keeping the $\mathcal{O}(\alpha_s)$ and $\mathcal{O}(\alpha_s^2)$ terms inside the curly bracket. For the numerical calculation, we choose $\alpha_s(m_Z) = 0.118$.

In the main text, we define the RG kernels in Eq. (2.34) and use them to express the resummed formula. Here we also provide the explicit expressions at different orders [123, 124]. For $S_\Gamma(\nu, \mu)$, we have

$$S_\Gamma(\nu, \mu) = S_\Gamma^{\text{LL}}(\nu, \mu) + S_\Gamma^{\text{NLL}}(\nu, \mu) + S_\Gamma^{\text{NNLL}}(\nu, \mu) + \dots \quad (\text{A.5})$$

with

$$\begin{aligned} S_\Gamma^{\text{LL}}(\nu, \mu) &= \frac{\Gamma_0 \pi}{\beta_0^2 \alpha_s(\nu)} \left(1 - \frac{1}{r} - \ln r \right), \\ S_\Gamma^{\text{NLL}}(\nu, \mu) &= \frac{\Gamma_0}{4\beta_0^2} \left[\left(\frac{\Gamma_1}{\Gamma_0} - \frac{\beta_1}{\beta_0} \right) (1 - r + \ln r) + \frac{\beta_1}{2\beta_0} \ln^2 r \right], \\ S_\Gamma^{\text{NNLL}}(\nu, \mu) &= \frac{\Gamma_0 \alpha_s(\nu)}{32\pi \beta_0^2} \left[\left(\frac{\beta_1^2}{\beta_0^2} - \frac{\beta_2}{\beta_0} \right) (1 - r^2 + 2 \ln r) + \left(\frac{\beta_1 \Gamma_1}{\beta_0 \Gamma_0} - \frac{\Gamma_2}{\Gamma_0} \right) (1 - r)^2 \right. \\ &\quad \left. + 2 \left(\frac{\beta_1 \Gamma_1}{\beta_0 \Gamma_0} - \frac{\beta_1^2}{\beta_0^2} \right) (1 - r + r \ln r) \right], \\ S_\Gamma^{\text{N}^3\text{LL}}(\nu, \mu) &= \frac{\Gamma_0 \alpha_s(\nu)^2}{64\pi^2 \beta_0^2} \left[\left(\frac{\beta_2}{\beta_0} - \frac{\beta_1^2}{\beta_0^2} \right) \left(\frac{\Gamma_1}{\Gamma_0} - \frac{\beta_1}{\beta_0} \right) \frac{(1-r)^2(2+r)}{3} + \left(\frac{\Gamma_3}{\Gamma_0} - \frac{\beta_3}{\beta_0} - \frac{\beta_1 \Gamma_2}{\beta_0 \Gamma_0} + \frac{\beta_1 \beta_2}{\beta_0^2} \right) \right. \\ &\quad \left(\frac{1-r^3}{3} - \frac{1-r^2}{2} \right) + \frac{\beta_1}{\beta_0} \left(\frac{\Gamma_2}{\Gamma_0} - \frac{\beta_2}{\beta_0} - \frac{\beta_1 \Gamma_1}{\beta_0 \Gamma_0} + \frac{\beta_1^2}{\beta_0^2} \right) \left(\frac{1-r^2}{4} + \frac{r^2 \ln r}{2} \right) \\ &\quad \left. + \left(-\frac{\beta_3}{\beta_0} + \frac{2\beta_1 \beta_2}{\beta_0^2} - \frac{\beta_1^3}{\beta_0^3} \right) \left(\frac{1-r^2}{4} + \frac{\ln r}{2} \right) \right]. \end{aligned} \quad (\text{A.6})$$

Here we define $r \equiv \frac{\alpha_s(\mu)}{\alpha_s(\nu)}$. Similarly, we have

$$\begin{aligned} A_\Gamma(\nu, \mu) &= A_\Gamma^{\text{LL}}(\nu, \mu) + A_\Gamma^{\text{NLL}}(\nu, \mu) + A_\Gamma^{\text{NNLL}}(\nu, \mu) + \dots, \\ A_{\gamma_j}(\nu, \mu) &= A_{\gamma_j}^{\text{LL}}(\nu, \mu) + A_{\gamma_j}^{\text{NLL}}(\nu, \mu) + A_{\gamma_j}^{\text{NNLL}}(\nu, \mu) + \dots. \end{aligned} \quad (\text{A.7})$$

The corresponding term at each order is

$$A_\Gamma^{\text{LL}}(\nu, \mu) = \frac{\Gamma_0}{2\beta_0} \ln r,$$

$$\begin{aligned}
A_{\Gamma}^{\text{NLL}}(\nu, \mu) &= \frac{\Gamma_0 \alpha_s(\nu)}{8\pi\beta_0} \left(\frac{\beta_1}{\beta_0} - \frac{\Gamma_1}{\Gamma_0} \right) (1-r), \\
A_{\Gamma}^{\text{NNLL}}(\nu, \mu) &= \frac{\Gamma_0 \alpha(\nu)^2}{64\pi^2\beta_0} \left(\frac{\beta_1^2}{\beta_0^2} - \frac{\beta_2}{\beta_0} + \frac{\Gamma_2}{\Gamma_0} - \frac{\beta_1\Gamma_1}{\beta_0\Gamma_0} \right) (r^2-1), \\
A_{\Gamma}^{\text{N}^3\text{LL}}(\nu, \mu) &= \frac{\Gamma_0 \alpha(\nu)^3}{384\pi^3\beta_0} \left[\frac{\Gamma_3}{\Gamma_0} - \frac{\Gamma_2\beta_1}{\Gamma_0\beta_0} + \frac{\Gamma_1}{\Gamma_0} \left(\frac{\beta_1^2}{\beta_0^2} - \frac{\beta_2}{\beta_0} \right) - \frac{\beta_1^3}{\beta_0^3} + \frac{2\beta_1\beta_2}{\beta_0^2} - \frac{\beta_3}{\beta_0} \right] (1-r^3)
\end{aligned} \quad (\text{A.8})$$

Expressions for $A_{\gamma_j}(\nu, \mu)$ are similar with the replacement of anomalous dimensions.

B Anomalous dimensions

In this section, we summarize all the anomalous dimensions needed for the resummation. First of all, the cusp anomalous dimension has been computed up to four loops in Ref. [125–131].

$$\gamma_{\text{cusp}}(\alpha_s) = \left(\frac{\alpha_s}{4\pi} \right) \Gamma_0 + \left(\frac{\alpha_s}{4\pi} \right)^2 \Gamma_1 + \left(\frac{\alpha_s}{4\pi} \right)^3 \Gamma_2 + \dots,$$

where [125, 126]

$$\begin{aligned}
\Gamma_0 &= 4, \\
\Gamma_1 &= 4 \left[C_A \left(\frac{67}{9} - \frac{\pi^2}{3} \right) - \frac{20}{9} T_F n_F \right], \\
\Gamma_2 &= 4 \left[\left(-\frac{56\zeta_3}{3} - \frac{418}{27} + \frac{40\pi^2}{27} \right) C_A n_f T_F + \left(\frac{22\zeta_3}{3} + \frac{245}{6} - \frac{134\pi^2}{27} + \frac{11\pi^4}{45} \right) C_A^2 \right. \\
&\quad \left. + \left(16\zeta_3 - \frac{55}{3} \right) C_F n_f T_F - \frac{16}{27} n_f^2 T_F^2 \right], \\
\Gamma_{3,q} &= 15526.5 - 3878.93 n_f + 146.683 n_f^2 + 2.454 n_f^3, \\
\Gamma_{3,g} &= 13626.7 - 3904.67 n_f + 146.683 n_f^2 + 2.454 n_f^3.
\end{aligned} \quad (\text{B.1})$$

For four-loop cusp Γ_3 , we only provide the numerical values and the full analytic result can be found in [130, 131]. Note that the Casimir scaling between quark and gluon cusp anomalous dimensions is broken at four-loop, and thus we give the values for both of them.

For the regular anomalous dimensions $\gamma[\alpha_s, \dots]$, with the dots representing potential dependence on kinematical variables, we also expand them in $\alpha_s/(4\pi)$,

$$\gamma[\alpha_s, \dots] = \sum_{n=0}^{\infty} \left(\frac{\alpha_s}{4\pi} \right)^{n+1} \gamma_n[\dots]. \quad (\text{B.2})$$

The quark and gluon anomalous dimensions through to three loops are [132–136]

$$\begin{aligned}
\gamma_0^q &= -3C_F, \\
\gamma_1^q &= C_A C_F \left(-11\zeta_2 + 26\zeta_3 - \frac{961}{54} \right) + C_F^2 \left(12\zeta_2 - 24\zeta_3 - \frac{3}{2} \right) + C_F n_f \left(2\zeta_2 + \frac{65}{27} \right), \\
\gamma_2^q &= -\frac{4880\pi^2\zeta_3}{81} + \frac{82072\zeta_3}{27} - \frac{15328\zeta_5}{9} - \frac{2066\pi^4}{405} - \frac{5062\pi^2}{81} - \frac{196621}{243}
\end{aligned}$$

$$\begin{aligned}
& + \left(-\frac{7472\zeta_3}{81} + \frac{68\pi^4}{1215} + \frac{4564\pi^2}{243} + \frac{36236}{729} \right) n_f + \left(-\frac{32\zeta_3}{81} - \frac{40\pi^2}{81} + \frac{9668}{2187} \right) n_f^2, \\
\gamma_0^g &= -\beta_0, \\
\gamma_1^g &= C_A^2 \left(\frac{11\zeta_2}{3} + 2\zeta_3 - \frac{692}{27} \right) + C_A n_f \left(\frac{128}{27} - \frac{2\zeta_2}{3} \right) + 2C_F n_f, \\
\gamma_2^g &= -60\pi^2\zeta_3 + 1098\zeta_3 - 432\zeta_5 - \frac{319\pi^4}{10} + \frac{6109\pi^2}{18} - \frac{97186}{27} \\
& + \left(\frac{460\zeta_3}{9} + \frac{107\pi^4}{45} - \frac{635\pi^2}{27} + \frac{59635}{162} \right) n_f + \left(-\frac{56\zeta_3}{9} + \frac{10\pi^2}{27} - \frac{1061}{486} \right) n_f^2. \quad (\text{B.3})
\end{aligned}$$

Next, The soft anomalous dimension up to three loops is [137]

$$\begin{aligned}
\gamma_0^s &= 0, \\
\gamma_1^s &= C_A \left(-\frac{808}{27} + \frac{22}{3}\zeta_2 + 28\zeta_3 \right) + n_f \left(\frac{112}{27} - \frac{4}{3}\zeta_2 \right), \\
\gamma_2^s &= C_A^2 \left(-\frac{136781}{729} + \frac{12650}{81}\zeta_2 + \frac{1316}{3}\zeta_3 - 176\zeta_4 - 192\zeta_5 - \frac{176}{3}\zeta_3\zeta_2 \right) \\
& + C_A n_f \left(\frac{11842}{729} - \frac{2828}{81}\zeta_2 - \frac{728}{27}\zeta_3 + 48\zeta_4 \right) \\
& + C_F n_f \left(\frac{1711}{27} - 4\zeta_2 - \frac{304}{9}\zeta_3 - 16\zeta_4 \right) + n_f^2 \left(\frac{2080}{729} + \frac{40}{27}\zeta_2 - \frac{112}{27}\zeta_3 \right). \quad (\text{B.4})
\end{aligned}$$

Finally, the rapidity anomalous dimension up to three loops is [79]

$$\begin{aligned}
\gamma_0^r &= 0, \\
\gamma_1^r &= C_A \left(-\frac{808}{27} + 28\zeta_3 \right) + n_f \frac{112}{27}, \\
\gamma_2^r &= C_A^2 \left(-\frac{297029}{729} + \frac{6392}{81}\zeta_2 + \frac{12328}{27}\zeta_3 + \frac{154}{3}\zeta_4 - 192\zeta_5 - \frac{176}{3}\zeta_3\zeta_2 \right) \\
& + C_A n_f \left(\frac{62626}{729} - \frac{824}{81}\zeta_2 - \frac{904}{27}\zeta_3 + \frac{20}{3}\zeta_4 \right) + n_f^2 \left(-\frac{1856}{729} - \frac{32}{9}\zeta_3 \right) \\
& + C_F n_f \left(\frac{1711}{27} - \frac{304}{9}\zeta_3 - 16\zeta_4 \right). \quad (\text{B.5})
\end{aligned}$$

C Fourier transformation

In this section, we derive the analytic transformation maps between logarithms in the Fourier and momentum space. Given the form in Eq. (2.52), we consider the following Fourier transformation convention

$$\mathcal{F} \left[\left(\frac{b_y \mu}{b_0} \right)^{2\epsilon} \right] \equiv \int_{-\infty}^{+\infty} \frac{db_y}{2\pi\xi} 2 \cos \left(\frac{b_y \tau_p}{\xi} \right) \left(\frac{b_y \mu}{b_0} \right)^{2\epsilon} = -\frac{2\Gamma(1+2\epsilon) \sin(\pi\epsilon)}{\pi \tau_p} \left(\frac{\mu \xi}{b_0 \tau_p} \right)^{2\epsilon} \quad (\text{C.1})$$

For convenience, we will define $x = \frac{2\tau_p}{\mu\xi}$, $L = \ln \left(\frac{b_y^2 \mu^2}{b_0^2} \right)$ and expand both sides in ϵ . Note that the right-hand side gives rise to the plus distributions in x while the left-hand side contains powers

of L . By mapping the coefficient in the same order of ϵ , we obtain the analytic expressions for the Fourier transformation relevant to the fixed-order expansion. The first few orders read

$$\begin{aligned}
\mathcal{F}[1] &= \frac{2}{\mu\xi} \delta(x), \\
\mathcal{F}[L] &= -\frac{4}{\mu\xi} \left[\frac{1}{x} \right]_+, \\
\mathcal{F}[L^2] &= \frac{2\pi^2}{3\mu\xi} \delta(x) + \frac{16}{\mu\xi} \left[\frac{\ln(x)}{x} \right]_+, \\
\mathcal{F}[L^3] &= -\frac{48}{\mu\xi} \left[\frac{\ln^2(x)}{x} \right]_+ - \frac{4\pi^2}{\mu\xi} \left[\frac{1}{x} \right]_+ - \frac{32\zeta_3}{\mu\xi} \delta(x), \\
\mathcal{F}[L^4] &= \frac{128}{\mu\xi} \left[\frac{\ln^3(x)}{x} \right]_+ + \frac{32\pi^2}{\mu\xi} \left[\frac{\ln(x)}{x} \right]_+ + \frac{256\zeta_3}{\mu\xi} \left[\frac{1}{x} \right]_+ + \frac{38\pi^4}{15\mu\xi} \delta(x), \\
\mathcal{F}[L^5] &= -\frac{320}{\mu\xi} \left[\frac{\ln^4(x)}{x} \right]_+ - \frac{160\pi^2}{\mu\xi} \left[\frac{\ln^2(x)}{x} \right]_+ - \frac{2560\zeta_3}{\mu\xi} \left[\frac{\ln(x)}{x} \right]_+ - \frac{76\pi^4}{3\mu\xi} \left[\frac{1}{x} \right]_+ \\
&\quad - \frac{64(5\pi^2\zeta_3 + 72\zeta_5)}{3\mu\xi} \delta(x). \tag{C.2}
\end{aligned}$$

D Fixed-order expansion

Here we provide the fixed-order expansion of the resummed formula in Eq. (2.52).

$$\frac{1}{\sigma_{\text{LO}}} \frac{d\sigma_q}{d\tau_p} = \int_T dv dw H_q^{(0)}(v, w) \left[\left(\frac{\alpha_s}{4\pi} \right) A_1(v, w, \tau_p) + \left(\frac{\alpha_s}{4\pi} \right)^2 A_2(v, w, \tau_p) + \mathcal{O}(\alpha_s^3) \right] \tag{D.1}$$

where the LO singular coefficient is

$$\begin{aligned}
A_1(v, w, \tau_p) &= -8(C_A + 2C_F) \frac{\ln\left(\frac{2\tau_p}{\xi Q}\right)}{\tau_p} \\
&\quad + \left(4C_A \ln\left(\frac{vw}{1-v-w}\right) - \frac{22C_A}{3} + 8C_F \ln(1-v-w) - 12C_F + \frac{8T_F n_F}{3} \right) \frac{1}{\tau_p} \tag{D.2}
\end{aligned}$$

and the NLO singular coefficient is

$$\begin{aligned}
A_2(v, w, \tau_p) &= 32(C_A + 2C_F)^2 \frac{\ln^3\left(\frac{2\tau_p}{\xi Q}\right)}{\tau_p} - (C_A + 2C_F) \left[48C_A \ln\left(\frac{vw}{1-v-w}\right) \right. \\
&\quad \left. + 96C_F \ln(1-v-w) - \frac{440}{3}C_A - 144C_F + \frac{160}{3}n_f T_F \right] \frac{\ln^2\left(\frac{2\tau_p}{\xi Q}\right)}{\tau_p} \\
&\quad + \left[-8(C_A + 2C_F) \frac{H_1(v, w)}{H_0(v, w)} + 16C_A^2 \ln^2\left(\frac{vw}{1-v-w}\right) \right. \\
&\quad \left. + (64C_F C_A \ln(1-v-w) - 88C_A^2 - 96C_F C_A + 32C_A T_F n_f) \ln\left(\frac{vw}{1-v-w}\right) \right. \\
&\quad \left. + 64C_F^2 \ln^2(1-v-w) - (176C_F C_A + 192C_F^2 - 64C_F T_F n_f) \ln(1-v-w) \right] \tag{D.3}
\end{aligned}$$

$$\begin{aligned}
& + \left(\frac{68}{3} C_A^2 + \frac{256}{3} C_F C_A + 80 C_F^2 \right) \pi^2 + \frac{172}{9} C_A^2 + \frac{208}{9} C_F C_A + 16 C_F^2 - 56 C_A T_F n_f \\
& - \frac{464}{9} C_F T_F n_f + \frac{128}{9} n_f^2 T_F^2 \right] \frac{\ln \left(\frac{2\tau_p}{\xi Q} \right)}{\tau_p} \\
& + \left[\frac{H_1(v, w)}{H_0(v, w)} \left(4C_A \ln \left(\frac{vw}{1-v-w} \right) + 8C_F \ln(1-v-w) - \frac{22}{3} C_A - 12C_F + \frac{8}{3} T_F n_f \right) \right. \\
& + \left(\left(-\frac{34}{3} C_A^2 - 20 C_F C_A \right) \pi^2 + \frac{389}{9} C_A^2 + 32 C_F C_A - \frac{100}{9} C_A T_F n_f \right) \ln \left(\frac{vw}{1-v-w} \right) \\
& + \left(\left(-40 C_F^2 - \frac{68}{3} C_F C_A \right) \pi^2 + 64 C_F^2 + \frac{796}{9} C_F C_A - \frac{200}{9} C_F T_F n_f \right) \ln(1-v-w) \\
& + \left(40 C_A^2 + 304 C_F C_A + 160 C_F^2 \right) \zeta_3 + \left(\frac{319}{9} C_A^2 + \frac{820}{9} C_F C_A + 68 C_F^2 - \frac{116}{9} C_A T_F n_f \right. \\
& \left. - \frac{200}{9} C_F T_F n_f \right) \pi^2 - \frac{2006}{27} C_A^2 - 172 C_F C_A - 102 C_F^2 + \frac{1028}{27} C_A T_F n_f + 60 C_F T_F n_f \\
& \left. - \frac{80}{27} n_f^2 T_F^2 \right] \frac{1}{\tau_p}. \tag{D.4}
\end{aligned}$$

Note that the $H_q^{(0)}(v, w)$ and $H_q^{(1)}(v, w)$ are the tree-level and one-loop hard function. $H_q^{(0)}(v, w)$ is given in Eq. (2.22), and $H_q^{(1)}(v, w)$ is provided in the ancillary file.

References

- [1] C. L. Basham, L. S. Brown, S. D. Ellis and S. T. Love, *Energy Correlations in electron-Positron Annihilation in Quantum Chromodynamics: Asymptotically Free Perturbation Theory*, *Phys. Rev. D* **19** (1979) 2018.
- [2] C. L. Basham, L. S. Brown, S. D. Ellis and S. T. Love, *Energy Correlations in electron - Positron Annihilation: Testing QCD*, *Phys. Rev. Lett.* **41** (1978) 1585.
- [3] H. Chen, M.-X. Luo, I. Moult, T.-Z. Yang, X. Zhang and H. X. Zhu, *Three point energy correlators in the collinear limit: symmetries, dualities and analytic results*, *JHEP* **08** (2020) 028 [[1912.11050](#)].
- [4] T. Kinoshita, *Mass singularities of Feynman amplitudes*, *J. Math. Phys.* **3** (1962) 650.
- [5] T. D. Lee and M. Nauenberg, *Degenerate Systems and Mass Singularities*, *Phys. Rev.* **133** (1964) B1549.
- [6] L. J. Dixon, M.-X. Luo, V. Shtabovenko, T.-Z. Yang and H. X. Zhu, *Analytical Computation of Energy-Energy Correlation at Next-to-Leading Order in QCD*, *Phys. Rev. Lett.* **120** (2018) 102001 [[1801.03219](#)].
- [7] M.-X. Luo, V. Shtabovenko, T.-Z. Yang and H. X. Zhu, *Analytic Next-To-Leading Order Calculation of Energy-Energy Correlation in Gluon-Initiated Higgs Decays*, *JHEP* **06** (2019) 037 [[1903.07277](#)].
- [8] J. Gao, V. Shtabovenko and T.-Z. Yang, *Energy-energy correlation in hadronic Higgs decays: analytic results and phenomenology at NLO*, *JHEP* **02** (2021) 210 [[2012.14188](#)].

- [9] A. V. Belitsky, S. Hohenegger, G. P. Korchemsky, E. Sokatchev and A. Zhiboedov, *From correlation functions to event shapes*, *Nucl. Phys. B* **884** (2014) 305 [[1309.0769](#)].
- [10] A. V. Belitsky, S. Hohenegger, G. P. Korchemsky, E. Sokatchev and A. Zhiboedov, *Event shapes in $\mathcal{N} = 4$ super-Yang-Mills theory*, *Nucl. Phys. B* **884** (2014) 206 [[1309.1424](#)].
- [11] A. V. Belitsky, S. Hohenegger, G. P. Korchemsky, E. Sokatchev and A. Zhiboedov, *Energy-Energy Correlations in $N=4$ Supersymmetric Yang-Mills Theory*, *Phys. Rev. Lett.* **112** (2014) 071601 [[1311.6800](#)].
- [12] J. M. Henn, E. Sokatchev, K. Yan and A. Zhiboedov, *Energy-energy correlation in $N=4$ super Yang-Mills theory at next-to-next-to-leading order*, *Phys. Rev. D* **100** (2019) 036010 [[1903.05314](#)].
- [13] T.-Z. Yang and X. Zhang, *Analytic Computation of three-point energy correlator in QCD*, *JHEP* **09** (2022) 006 [[2208.01051](#)].
- [14] T.-Z. Yang and X. Zhang, *Three-point energy correlators in hadronic Higgs boson decays*, *Phys. Rev. D* **109** (2024) 114036 [[2402.05174](#)].
- [15] K. Yan and X. Zhang, *Three-Point Energy Correlator in $N=4$ Supersymmetric Yang-Mills Theory*, *Phys. Rev. Lett.* **129** (2022) 021602 [[2203.04349](#)].
- [16] D. Chicherin, I. Moult, E. Sokatchev, K. Yan and Y. Zhu, *The Collinear Limit of the Four-Point Energy Correlator in $\mathcal{N} = 4$ Super Yang-Mills Theory*, [2401.06463](#).
- [17] L. J. Dixon, I. Moult and H. X. Zhu, *Collinear limit of the energy-energy correlator*, *Phys. Rev. D* **100** (2019) 014009 [[1905.01310](#)].
- [18] G. P. Korchemsky, *Energy correlations in the end-point region*, *JHEP* **01** (2020) 008 [[1905.01444](#)].
- [19] J. C. Collins and D. E. Soper, *Back-to-back jets in qcd*, *Nuclear Physics B* **193** (1981) 381.
- [20] S. Ellis, D. Richards and W. Stirling, *Fixed order perturbation theory and leading logarithms in energy-energy correlations*, *Physics Letters B* **136** (1984) 99.
- [21] D. de Florian and M. Grazzini, *The Back-to-back region in $e+ e-$ energy-energy correlation*, *Nucl. Phys. B* **704** (2005) 387 [[hep-ph/0407241](#)].
- [22] Z. Tulipánt, A. Kardos and G. Somogyi, *Energy-energy correlation in electron-positron annihilation at NNLL + NNLO accuracy*, *Eur. Phys. J. C* **77** (2017) 749 [[1708.04093](#)].
- [23] I. Moult and H. X. Zhu, *Simplicity from Recoil: The Three-Loop Soft Function and Factorization for the Energy-Energy Correlation*, *JHEP* **08** (2018) 160 [[1801.02627](#)].
- [24] I. Moult, G. Vita and K. Yan, *Subleading power resummation of rapidity logarithms: the energy-energy correlator in $\mathcal{N} = 4$ SYM*, *JHEP* **07** (2020) 005 [[1912.02188](#)].
- [25] M. A. Ebert, B. Mistlberger and G. Vita, *The Energy-Energy Correlation in the back-to-back limit at N^3LO and N^3LL'* , *JHEP* **08** (2021) 022 [[2012.07859](#)].
- [26] I. Moult, H. X. Zhu and Y. J. Zhu, *The Four Loop QCD Rapidity Anomalous Dimension*, [2205.02249](#).
- [27] C. Duhr, B. Mistlberger and G. Vita, *The Four-Loop Rapidity Anomalous Dimension and Event Shapes to Fourth Logarithmic Order*, [2205.02242](#).
- [28] A. Gao, H. T. Li, I. Moult and H. X. Zhu, *Precision QCD Event Shapes at Hadron Colliders: The Transverse Energy-Energy Correlator in the Back-to-Back Limit*, *Phys. Rev. Lett.* **123** (2019) 062001 [[1901.04497](#)].

- [29] A. Gao, H. T. Li, I. Moult and H. X. Zhu, *The transverse energy-energy correlator at next-to-next-to-next-to-leading logarithm*, *JHEP* **09** (2024) 072 [2312.16408].
- [30] H. Chen, I. Moult, X. Zhang and H. X. Zhu, *Rethinking jets with energy correlators: Tracks, resummation, and analytic continuation*, *Phys. Rev. D* **102** (2020) 054012 [2004.11381].
- [31] K. Lee, B. Meçaj and I. Moult, *Conformal Colliders Meet the LHC*, 2205.03414.
- [32] W. Chen, J. Gao, Y. Li, Z. Xu, X. Zhang and H. X. Zhu, *NNLL resummation for projected three-point energy correlator*, *JHEP* **05** (2024) 043 [2307.07510].
- [33] K. Lee, I. Moult and X. Zhang, *Revisiting Single Inclusive Jet Production: Timelike Factorization and Reciprocity*, 2409.19045.
- [34] CMS collaboration, *Measurement of Energy Correlators inside Jets and Determination of the Strong Coupling $\alpha S(mZ)$* , *Phys. Rev. Lett.* **133** (2024) 071903 [2402.13864].
- [35] S. Catani, Y. L. Dokshitzer, M. Olsson, G. Turnock and B. R. Webber, *New clustering algorithm for multi - jet cross-sections in e+ e- annihilation*, *Phys. Lett. B* **269** (1991) 432.
- [36] A. Banfi, Y. L. Dokshitzer, G. Marchesini and G. Zanderighi, *QCD analysis of D parameter in near to planar three jet events*, *JHEP* **05** (2001) 040 [hep-ph/0104162].
- [37] L. Arpino, A. Banfi and B. K. El-Menoufi, *Near-to-planar three-jet events at NNLL accuracy*, *JHEP* **07** (2020) 171 [1912.09341].
- [38] S. Catani and M. H. Seymour, *The Dipole formalism for the calculation of QCD jet cross-sections at next-to-leading order*, *Phys. Lett. B* **378** (1996) 287 [hep-ph/9602277].
- [39] S. Catani and M. H. Seymour, *A General algorithm for calculating jet cross-sections in NLO QCD*, *Nucl. Phys. B* **485** (1997) 291 [hep-ph/9605323].
- [40] Z. Nagy and Z. Trocsanyi, *Next-to-leading order calculation of four jet observables in electron positron annihilation*, *Phys. Rev. D* **59** (1999) 014020 [hep-ph/9806317].
- [41] C. W. Bauer, S. Fleming and M. E. Luke, *Summing Sudakov logarithms in $B \rightarrow X_s \gamma$ in effective field theory.*, *Phys. Rev. D* **63** (2000) 014006 [hep-ph/0005275].
- [42] C. W. Bauer, S. Fleming, D. Pirjol and I. W. Stewart, *An Effective field theory for collinear and soft gluons: Heavy to light decays*, *Phys. Rev. D* **63** (2001) 114020 [hep-ph/0011336].
- [43] C. W. Bauer and I. W. Stewart, *Invariant operators in collinear effective theory*, *Phys. Lett. B* **516** (2001) 134 [hep-ph/0107001].
- [44] C. W. Bauer, D. Pirjol and I. W. Stewart, *Soft collinear factorization in effective field theory*, *Phys. Rev. D* **65** (2002) 054022 [hep-ph/0109045].
- [45] A. Gehrmann-De Ridder, T. Gehrmann, E. W. N. Glover and G. Heinrich, *NNLO corrections to event shapes in e+ e- annihilation*, *JHEP* **12** (2007) 094 [0711.4711].
- [46] A. Gehrmann-De Ridder, T. Gehrmann, E. W. N. Glover and G. Heinrich, *Second-order QCD corrections to the thrust distribution*, *Phys. Rev. Lett.* **99** (2007) 132002 [0707.1285].
- [47] T. Becher and M. D. Schwartz, *A precise determination of α_s from LEP thrust data using effective field theory*, *JHEP* **07** (2008) 034 [0803.0342].
- [48] R. Abbate, M. Fickinger, A. H. Hoang, V. Mateu and I. W. Stewart, *Thrust at $N^3 LL$ with Power Corrections and a Precision Global Fit for $\alpha_s(mZ)$* , *Phys. Rev. D* **83** (2011) 074021 [1006.3080].

- [49] M. A. Benitez-Rathgeb, A. H. Hoang, V. Mateu, I. W. Stewart and G. Vita, *Determining $\alpha_s(m_Z)$ from Thrust with Power Corrections*, in *58th Rencontres de Moriond on QCD and High Energy Interactions*, 5, 2024, [2405.14380](#).
- [50] G. P. Salam and D. Wicke, *Hadron masses and power corrections to event shapes*, *JHEP* **05** (2001) 061 [[hep-ph/0102343](#)].
- [51] Y.-T. Chien and M. D. Schwartz, *Resummation of heavy jet mass and comparison to LEP data*, *JHEP* **08** (2010) 058 [[1005.1644](#)].
- [52] Z. Nagy and Z. Trocsanyi, *Next-to-leading order calculation of four jet shape variables*, *Phys. Rev. Lett.* **79** (1997) 3604 [[hep-ph/9707309](#)].
- [53] J. M. Campbell, M. A. Cullen and E. W. N. Glover, *Four jet event shapes in electron - positron annihilation*, *Eur. Phys. J. C* **9** (1999) 245 [[hep-ph/9809429](#)].
- [54] A. Banfi, G. Marchesini, Y. L. Dokshitzer and G. Zanderighi, *QCD analysis of near-to-planar three jet events*, *JHEP* **07** (2000) 002 [[hep-ph/0004027](#)].
- [55] A. Banfi, Y. L. Dokshitzer, G. Marchesini and G. Zanderighi, *Near-to-planar three jet events in and beyond QCD perturbation theory*, *Phys. Lett. B* **508** (2001) 269 [[hep-ph/0010267](#)].
- [56] A. Banfi, Y. L. Dokshitzer, G. Marchesini and G. Zanderighi, *Nonperturbative QCD analysis of near - to - planar three jet events*, *JHEP* **03** (2001) 007 [[hep-ph/0101205](#)].
- [57] A. J. Larkoski and A. Procita, *New Insights on an Old Problem: Resummation of the D-parameter*, *JHEP* **02** (2019) 104 [[1810.06563](#)].
- [58] A. Bhattacharya, M. D. Schwartz and X. Zhang, *Sudakov shoulder resummation for thrust and heavy jet mass*, *Phys. Rev. D* **106** (2022) 074011 [[2205.05702](#)].
- [59] A. Bhattacharya, J. K. L. Michel, M. D. Schwartz, I. W. Stewart and X. Zhang, *NNLL resummation of Sudakov shoulder logarithms in the heavy jet mass distribution*, *JHEP* **11** (2023) 080 [[2306.08033](#)].
- [60] G. Luisoni, P. F. Monni and G. P. Salam, *C-parameter hadronisation in the symmetric 3-jet limit and impact on α_s fits*, *Eur. Phys. J. C* **81** (2021) 158 [[2012.00622](#)].
- [61] F. Caola, S. Ferrario Ravasio, G. Limatola, K. Melnikov and P. Nason, *On linear power corrections in certain collider observables*, *JHEP* **01** (2022) 093 [[2108.08897](#)].
- [62] F. Caola, S. Ferrario Ravasio, G. Limatola, K. Melnikov, P. Nason and M. A. Ozcelik, *Linear power corrections to e^+e^- shape variables in the three-jet region*, *JHEP* **12** (2022) 062 [[2204.02247](#)].
- [63] P. Nason and G. Zanderighi, *Fits of α_s using power corrections in the three-jet region*, *JHEP* **06** (2023) 058 [[2301.03607](#)].
- [64] CEPC STUDY GROUP collaboration, *CEPC Conceptual Design Report: Volume 1 - Accelerator*, [1809.00285](#).
- [65] CEPC STUDY GROUP collaboration, *CEPC Conceptual Design Report: Volume 2 - Physics & Detector*, [1811.10545](#).
- [66] CEPC STUDY GROUP collaboration, *CEPC Technical Design Report – Accelerator*, [2312.14363](#).
- [67] T. Behnke, J. E. Brau, B. Foster, J. Fuster, M. Harrison, J. M. Paterson et al., *The International Linear Collider Technical Design Report - Volume 1: Executive Summary*, [1306.6327](#).
- [68] ILC collaboration, *The International Linear Collider Technical Design Report - Volume 2: Physics*, [1306.6352](#).

- [69] TLEP DESIGN STUDY WORKING GROUP collaboration, *First Look at the Physics Case of TLEP*, *JHEP* **01** (2014) 164 [[1308.6176](#)].
- [70] J. Holguin, I. Moult, A. Pathak and M. Procura, *New paradigm for precision top physics: Weighing the top with energy correlators*, *Phys. Rev. D* **107** (2023) 114002 [[2201.08393](#)].
- [71] J. Holguin, I. Moult, A. Pathak, M. Procura, R. Schöfbeck and D. Schwarz, *Using the W as a Standard Candle to Reach the Top: Calibrating Energy Correlator Based Top Mass Measurements*, [2311.02157](#).
- [72] M. Xiao, Y. Ye and X. Zhu, *Prospect of measuring the top quark mass through energy correlators*, [2405.20001](#).
- [73] J. Holguin, I. Moult, A. Pathak, M. Procura, R. Schöfbeck and D. Schwarz, *Top Quark Mass Extractions from Energy Correlators: A Feasibility Study*, [2407.12900](#).
- [74] A. Pathak, “Using the W as a Standard Candle to Reach the Top.” https://agenda.infn.it/event/37093/contributions/234277/attachments/124186/182513/Aditya_Pathak_Boost_24.pdf, 2024.
- [75] L. J. Dixon and A. Signer, *Complete O(alpha-s**3) results for e+ e- —> (gamma, Z) —> four jets*, *Phys. Rev. D* **56** (1997) 4031 [[hep-ph/9706285](#)].
- [76] J. Collins, *Foundations of Perturbative QCD*, vol. 32 of *Cambridge Monographs on Particle Physics, Nuclear Physics and Cosmology*. Cambridge University Press, 7, 2023, [10.1017/9781009401845](#).
- [77] M.-X. Luo, X. Wang, X. Xu, L. L. Yang, T.-Z. Yang and H. X. Zhu, *Transverse Parton Distribution and Fragmentation Functions at NNLO: the Quark Case*, *JHEP* **10** (2019) 083 [[1908.03831](#)].
- [78] M.-X. Luo, T.-Z. Yang, H. X. Zhu and Y. J. Zhu, *Transverse Parton Distribution and Fragmentation Functions at NNLO: the Gluon Case*, *JHEP* **01** (2020) 040 [[1909.13820](#)].
- [79] Y. Li and H. X. Zhu, *Bootstrapping Rapidity Anomalous Dimensions for Transverse-Momentum Resummation*, *Phys. Rev. Lett.* **118** (2017) 022004 [[1604.01404](#)].
- [80] A. A. Vladimirov, *Correspondence between Soft and Rapidity Anomalous Dimensions*, *Phys. Rev. Lett.* **118** (2017) 062001 [[1610.05791](#)].
- [81] L. W. Garland, T. Gehrmann, E. W. N. Glover, A. Koukoutsakis and E. Remiddi, *The Two loop QCD matrix element for e+ e- —> 3 jets*, *Nucl. Phys. B* **627** (2002) 107 [[hep-ph/0112081](#)].
- [82] L. W. Garland, T. Gehrmann, E. W. N. Glover, A. Koukoutsakis and E. Remiddi, *Two loop QCD helicity amplitudes for e+ e- —> three jets*, *Nucl. Phys. B* **642** (2002) 227 [[hep-ph/0206067](#)].
- [83] T. Gehrmann, P. Jakubčík, C. C. Mella, N. Syrrakos and L. Tancredi, *Two-loop helicity amplitudes for V+jet production including axial vector couplings to higher orders in epsilon*, *JHEP* **09** (2023) 192 [[2306.10170](#)].
- [84] S. Catani, *The Singular behavior of QCD amplitudes at two loop order*, *Phys. Lett. B* **427** (1998) 161 [[hep-ph/9802439](#)].
- [85] T. Becher and M. Neubert, *Infrared singularities of scattering amplitudes in perturbative QCD*, *Phys. Rev. Lett.* **102** (2009) 162001 [[0901.0722](#)].
- [86] T. Becher and M. Neubert, *On the Structure of Infrared Singularities of Gauge-Theory Amplitudes*, *JHEP* **06** (2009) 081 [[0903.1126](#)].

- [87] E. Gardi and L. Magnea, *Factorization constraints for soft anomalous dimensions in QCD scattering amplitudes*, *JHEP* **03** (2009) 079 [[0901.1091](#)].
- [88] O. Almelid, C. Duhr and E. Gardi, *Three-loop corrections to the soft anomalous dimension in multileg scattering*, *Phys. Rev. Lett.* **117** (2016) 172002 [[1507.00047](#)].
- [89] O. Almelid, C. Duhr, E. Gardi, A. McLeod and C. D. White, *Bootstrapping the QCD soft anomalous dimension*, *JHEP* **09** (2017) 073 [[1706.10162](#)].
- [90] M.-x. Luo, T.-Z. Yang, H. X. Zhu and Y. J. Zhu, *Unpolarized quark and gluon TMD PDFs and FFs at N^3LO* , *JHEP* **06** (2021) 115 [[2012.03256](#)].
- [91] M. A. Ebert, B. Mistlberger and G. Vita, *TMD fragmentation functions at N^3LO* , *JHEP* **07** (2021) 121 [[2012.07853](#)].
- [92] J. G. M. Gatheral, *Exponentiation of Eikonal Cross-sections in Nonabelian Gauge Theories*, *Phys. Lett. B* **133** (1983) 90.
- [93] J. Frenkel and J. C. Taylor, *NONABELIAN EIKONAL EXPONENTIATION*, *Nucl. Phys. B* **246** (1984) 231.
- [94] S. Catani, D. Colferai and A. Torrini, *Triple (and quadruple) soft-gluon radiation in QCD hard scattering*, *JHEP* **01** (2020) 118 [[1908.01616](#)].
- [95] T. Hahn, *CUBA: A Library for multidimensional numerical integration*, *Comput. Phys. Commun.* **168** (2005) 78 [[hep-ph/0404043](#)].
- [96] D. Kahaner, E. de Doncker-Kapenga, C. W. Überhuber and R. Piessens, *Quadpack*, in *Quadpack*, (Germany), Springer Berlin / Heidelberg, (1983).
- [97] T. Ooura and M. Mori, *The double exponential formula for oscillatory functions over the half infinite interval*, *Journal of Computational and Applied Mathematics* **38** (1991) 353.
- [98] M. e. a. Galassi, *Gnu scientific library reference manual*, 2018.
- [99] Y. Wang, L. L. Yang and B. Zhou, *FastGPL: a C++ library for fast evaluation of generalized polylogarithms*, [2112.04122](#).
- [100] T. Becher, A. Broggio and A. Ferroglio, *Introduction to Soft-Collinear Effective Theory*, vol. 896. Springer, 2015, [10.1007/978-3-319-14848-9](#), [[1410.1892](#)].
- [101] I. W. Stewart, F. J. Tackmann, J. R. Walsh and S. Zuberi, *Jet p_T resummation in Higgs production at NNLL' + NNLO*, *Phys. Rev. D* **89** (2014) 054001 [[1307.1808](#)].
- [102] M. L. Laursen, K. O. Mikaelian and M. A. Samuel, *ELECTRON - POSITRON ANNIHILATION INTO THREE GLUONS*, *Phys. Rev. D* **25** (1982) 710.
- [103] Baier, V N and Kurayev, E A and Fadin, V S, *Production of gluon jets in $e+e-$ collisions*, *Sov. J. Nucl. Phys.* **31(3)** (1980) 364.
- [104] T. Sjöstrand, S. Ask, J. R. Christiansen, R. Corke, N. Desai, P. Ilten et al., *An introduction to PYTHIA 8.2*, *Comput. Phys. Commun.* **191** (2015) 159 [[1410.3012](#)].
- [105] M. Beneke, *Renormalons*, *Phys. Rept.* **317** (1999) 1 [[hep-ph/9807443](#)].
- [106] C. Lee and G. F. Sterman, *Momentum Flow Correlations from Event Shapes: Factorized Soft Gluons and Soft-Collinear Effective Theory*, *Phys. Rev. D* **75** (2007) 014022 [[hep-ph/0611061](#)].
- [107] A. H. Hoang and I. W. Stewart, *Designing gapped soft functions for jet production*, *Phys. Lett. B* **660** (2008) 483 [[0709.3519](#)].

- [108] M. Cacciari, G. P. Salam and G. Soyez, *FastJet User Manual*, *Eur. Phys. J. C* **72** (2012) 1896 [[1111.6097](#)].
- [109] G. Parisi, *Super Inclusive Cross-Sections*, *Phys. Lett. B* **74** (1978) 65.
- [110] J. F. Donoghue, F. Low and S.-Y. Pi, *Tensor Analysis of Hadronic Jets in Quantum Chromodynamics*, *Phys. Rev. D* **20** (1979) 2759.
- [111] R. Ellis, D. Ross and A. Terrano, *The Perturbative Calculation of Jet Structure in $e+e-$ Annihilation*, *Nucl. Phys. B* **178** (1981) 421.
- [112] M. Dasgupta and G. P. Salam, *Event shapes in $e+e-$ annihilation and deep inelastic scattering*, *J. Phys. G* **30** (2004) R143 [[hep-ph/0312283](#)].
- [113] H. Chen, I. Moult and H. X. Zhu, *Quantum Interference in Jet Substructure from Spinning Gluons*, *Phys. Rev. Lett.* **126** (2021) 112003 [[2011.02492](#)].
- [114] H. Chen, I. Moult and H. X. Zhu, *Spinning gluons from the QCD light-ray OPE*, *JHEP* **08** (2022) 233 [[2104.00009](#)].
- [115] H. Chen, I. Moult, J. Sandor and H. X. Zhu, *Celestial blocks and transverse spin in the three-point energy correlator*, *JHEP* **09** (2022) 199 [[2202.04085](#)].
- [116] H. Chen, X. Zhou and H. X. Zhu, *Power corrections to energy flow correlations from large spin perturbation*, *JHEP* **10** (2023) 132 [[2301.03616](#)].
- [117] H. Chen, *QCD factorization from light-ray OPE*, *JHEP* **01** (2024) 035 [[2311.00350](#)].
- [118] H. Chen, P. F. Monni, Z. Xu and H. X. Zhu, *Scaling violation in power corrections to energy correlators from the light-ray OPE*, [2406.06668](#).
- [119] O. V. Tarasov, A. A. Vladimirov and A. Y. Zharkov, *The Gell-Mann-Low Function of QCD in the Three Loop Approximation*, *Phys. Lett. B* **93** (1980) 429.
- [120] S. A. Larin and J. A. M. Vermaseren, *The Three loop QCD Beta function and anomalous dimensions*, *Phys. Lett. B* **303** (1993) 334 [[hep-ph/9302208](#)].
- [121] T. van Ritbergen, J. A. M. Vermaseren and S. A. Larin, *The Four loop beta function in quantum chromodynamics*, *Phys. Lett. B* **400** (1997) 379 [[hep-ph/9701390](#)].
- [122] M. Czakon, *The Four-loop QCD beta-function and anomalous dimensions*, *Nucl. Phys. B* **710** (2005) 485 [[hep-ph/0411261](#)].
- [123] S. W. Bosch, R. J. Hill, B. O. Lange and M. Neubert, *Factorization and Sudakov resummation in leptonic radiative B decay*, *Phys. Rev. D* **67** (2003) 094014 [[hep-ph/0301123](#)].
- [124] M. Neubert, *Renormalization-group improved calculation of the $B \rightarrow X(s)$ gamma branching ratio*, *Eur. Phys. J. C* **40** (2005) 165 [[hep-ph/0408179](#)].
- [125] G. P. Korchemsky and A. V. Radyushkin, *Renormalization of the Wilson Loops Beyond the Leading Order*, *Nucl. Phys. B* **283** (1987) 342.
- [126] S. Moch, J. A. M. Vermaseren and A. Vogt, *The Three loop splitting functions in QCD: The Nonsinglet case*, *Nucl. Phys. B* **688** (2004) 101 [[hep-ph/0403192](#)].
- [127] S. Moch, B. Ruijl, T. Ueda, J. A. M. Vermaseren and A. Vogt, *Four-Loop Non-Singlet Splitting Functions in the Planar Limit and Beyond*, *JHEP* **10** (2017) 041 [[1707.08315](#)].
- [128] S. Moch, B. Ruijl, T. Ueda, J. A. M. Vermaseren and A. Vogt, *On quartic colour factors in splitting functions and the gluon cusp anomalous dimension*, *Phys. Lett. B* **782** (2018) 627 [[1805.09638](#)].

- [129] J. Davies, A. Vogt, B. Ruijl, T. Ueda and J. A. M. Vermaseren, *Large- nf contributions to the four-loop splitting functions in QCD*, *Nucl. Phys. B* **915** (2017) 335 [[1610.07477](#)].
- [130] J. M. Henn, G. P. Korchemsky and B. Mistlberger, *The full four-loop cusp anomalous dimension in $\mathcal{N} = 4$ super Yang-Mills and QCD*, *JHEP* **04** (2020) 018 [[1911.10174](#)].
- [131] A. von Manteuffel, E. Panzer and R. M. Schabinger, *Cusp and collinear anomalous dimensions in four-loop QCD from form factors*, *Phys. Rev. Lett.* **124** (2020) 162001 [[2002.04617](#)].
- [132] S. Moch, J. A. M. Vermaseren and A. Vogt, *The Quark form-factor at higher orders*, *JHEP* **08** (2005) 049 [[hep-ph/0507039](#)].
- [133] S. Moch, J. A. M. Vermaseren and A. Vogt, *Three-loop results for quark and gluon form-factors*, *Phys. Lett. B* **625** (2005) 245 [[hep-ph/0508055](#)].
- [134] A. Idilbi, X.-d. Ji, J.-P. Ma and F. Yuan, *Threshold resummation for Higgs production in effective field theory*, *Phys. Rev. D* **73** (2006) 077501 [[hep-ph/0509294](#)].
- [135] A. Idilbi, X.-d. Ji and F. Yuan, *Resummation of threshold logarithms in effective field theory for DIS, Drell-Yan and Higgs production*, *Nucl. Phys. B* **753** (2006) 42 [[hep-ph/0605068](#)].
- [136] T. Becher, M. Neubert and B. D. Pecjak, *Factorization and Momentum-Space Resummation in Deep-Inelastic Scattering*, *JHEP* **01** (2007) 076 [[hep-ph/0607228](#)].
- [137] Y. Li, A. von Manteuffel, R. M. Schabinger and H. X. Zhu, *Soft-virtual corrections to Higgs production at N^3LO* , *Phys. Rev. D* **91** (2015) 036008 [[1412.2771](#)].